DEVELOPMENT OF WINDBREAKS AS A DUST CONTROL STRATEGY FOR COMMUNITIES IN ARID CLIMATES SUCH AS THE US-MEXICO BORDER REGION

SCERP PROJECT NUMBER: A-04-06

ERIC R. PARDYJAK, UNIVERSITY OF UTAH

PRATHAP RAMAMURTHY, UNIVERSITY OF UTAH

SCOTT SPECKART, UNIVERSITY OF UTAH

INTRODUCTION

Reduction of fugitive dust emissions in arid regions such as those in the US-Mexico border region is of utmost concern to border air quality. Known as fugitive dust, particulate matter generated from the mechanical disturbance of granular crustal material has many sources and is a serious health concern. Sources include but are not limited to: Unpaved roads, construction operations, grazing land, agriculture and mine tailings. PM_{10} is the criteria pollutant commonly associated with fugitive dust and has been linked with numerous health problems. Illnesses can include lung and heart disease to asthma. Severity can vary from chronic health nuisances to death (Samet et al. 1998). Because it is not emitted as part of a regulated airstream, reductions in fugitive dust emissions have proven difficult. Air quality officials in the southwest are dissatisfied with the available options for controlling vehicle generated fugitive dust since water-based treatments are often impractical in arid climates. Previous SCERP-funded studies in Doña Ana County, New Mexico have examined the hypothesis that dust traveling near the ground is redeposited when it encounters brush, fences, and small terrain irregularities. A conclusion from this work is that depending upon atmospheric stability (i.e. time of day), vegetative canopies may affect the amount of vehicle-suspended dust that is actually transported sufficient distance to affect local and regional air quality. Other field studies have supported this conclusion. This study seeks to observe if similar results are obtained with an artificial windbreak. The first portion of this report describes windbreak results from a field experiment in Nogales, Sonora, while Appendices 1 and 2 describes the details of a numerical model designed to predict deposition for a wide range of rough surfaces.

RESEARCH OBJECTIVES

The research documented in this report covers a field experiment performed in Nogales, Sonora during the month of May 2006. This experiment uses automotive traffic on an unpaved road as a source of fugitive dust. A computer simulation code that models dust traveling downwind of a dirt road is used as well to describe the characteristics of dust transport in an artificial windbreak. This model is described thoroughly by Pardyjak et al. (submitted October 2007), and, Veranth et al. (submitted Oct. 2007) and are included at the end of this document. Other methods of describing dust transport, such as Gaussian Plume models, and mass fraction advected down wind are utilized. The latter method has been used by Veranth et al. (2003) and Etyemezian et al. (2004).

An objective is to obtain a greater understanding of the principles that one may use to implement an artificial windbreak dust control strategy. Issues such as height and number of rows of windbreaks will be explored. An evaluation of effectiveness of specific dust control strategies is the final objective of this work.

RESEARCH METHODOLOGY/ APPROACHES

Background

The motivation for the use of vegetative canopies or artificial windbreaks is shown in figure 1. On the left of the figure there is an undisturbed mean velocity profile with wind speeds that typically vary vertically in a logarithmic manner. As the wind encounters vegetation, buildings or an artificial wind break the air near these obstructions slows down and depending on the type of flow the velocity profile takes on a drastically different character. In figure 1a the velocity profile below the vegetative canopy top takes on an exponential profile as noted in Cionco (1965). The new modified exponential profile is deficit in momentum near these obstacles. Similar profiles are observed downwind of windbreaks with low porosity, $\phi < 0.2$, (Fig 1c), while windbreaks with high solidity, (Fig 1b), have recirculating flow with associated strong down ward velocities and reattachment point (McNaughton, 1988).

As wind or vehicles disturb granular material, fugitive dust is emitted into the air stream. If the fugitive dust is emitted into an undisturbed, high momentum logarithmic profile, its residence time near the ground or small obstacles, such as vines or sparse grass will be small (i.e. the PM is quickly advected away and diluted). As a consequence the probability of an appreciable quantity of fugitive dust being redeposited to the ground or small obstacles is small compared to a vegetated case.

If the dust is emitted into a slower, highly turbulent, modified exponential profile, the residence time of the dust spent near the ground and other obstacles is much greater thus increasing the probability that a significant amount of dust is redeposited. It is also probable that the concentration of dust in a vegetative canopy or an artificial windbreak would be higher than the air directly above due to this increased residence time characteristic of canopies and wind breaks.

Additional factors also modify fugitive dust transport. For example, dust needs a physical surface for redeposition. Vegetative canopies and artificial wind breaks provide additional surface area for redeposition. Another important factor is atmospheric stability. If the atmosphere is unstable vertical mixing will be promoted. The distribution of the cloud will reach higher elevations far above obstructions and ground. Under these circumstances a lower fraction of fugitive dust would be expected to be redeposited. The converse would be true for stable conditions. Experimentally, this has been observed by three separate experiments. One of these experiments is documented in Veranth et al. (2003) another in Etyemezian et al. (2004) and the final in Veranth et al. (2007).

Experiment Description

The May 2006 Nogales Sonora experiment was performed on the dates of May 25, 28, and 29. These dates corresponded with experiments that contained no fence, a 1 m high fence, and a two meter high fence. This is summarized with times and rate of vehicle traffic in Table 1.Theses dates were determined primarily by meteorological conditions and secondarily by equipment status. The location of the experiment was the Nogales Campus of El Colegio Nacional de Educación Professional Técnica (CONALEP) secondary technical school system. (N 31° 16.644’ W 110° 56.694’). It is located in the southern third of the metropolitan area of Nogales, about 200 or 300 m to the west of the principle street that bisects Nogales. Located to the west and up hill of CONALEP is an unpaved road that is the only access to a large and growing *colonia* (neighborhood). During the morning and evening rush hours, especially the evening, the CONALEP campus is subject to high levels of fugitive dust from the road. For these reasons, as well as establishing Mexican Collaboration, this site was chosen. The site was characterized as arid with short grasses, about 20-60 cm, for about 10 m downwind of the road.

The experimental set up is shown in figure 2. During the experiment runs the site had winds predominantly from west, south west. After traveling over the unpaved road the dust rich air was intercepted by an array of TSI inc. Dustraks and Campbell Scientific CSAT3 sonic anemometers. The artificial windbreak was an event ski fence from REILIBLE RACING INC, that had an optical porosity = 0.53. It was built using bamboo sticks from the same company. The bamboo sticks were driven into the ground with metal posts. The fence extended 92.2 m to the south and 91.4 m to the north of the half plane containing the ultrasonic anemometers and Dustraks. The physical location of the Dustraks and sonic anemometers is located in Table 2. The Dustraks were equipped with PM_{10} inlets and sampled at a rate of 1Hz. The Sonic anemometers sampled at a rate of 10 Hz. The artificial wind break was located between the first two Dustrak towers. The first Dustrak tower provided data that indicated the magnitude of dust initial suspended. Location was as close to the road as possible without imposing a safety hazard.

The second tower of Dustraks was less than half a meter from the back (downwind face) of the artificial windbreak. This close location was chosen to provide an accurate concentration data directly behind the windbreak. A 5 m Aluminum tower housed the three ultrasonic anemometers along with two other Dustraks. A final Dustrak tower was located at the downwind side of the test site. Similar configurations were used in the in Veranth et al. (2003) the Etyemezian et al. (2004) and Pardyjak et al. (2006) experiments.

There are many meteorological conditions that must be satisfied to have a successful experiment. One the principle wind direction must be within 60° of flowing perpendicular to the road. The 2 m fence experiment was 20 minutes shorter than the other two experiments because this 60° rule was violated during the final 20 minutes. Another involves the magnitude of wind. A high wind, about 15-20 m/s will suspend dust from sources other than the road. Under these conditions quantifying the effectiveness a windbreak or vegetative canopy would be extremely difficult if not impossible. High winds may also generate erroneous sonic anemometer measurements. Lastly precipitation may greatly reduces the amount of dust suspended by cars, or eliminate it completely.

Owing to the high amount of motor traffic, a continuous line source was assumed in the analysis. The topographical changes in the direction along the road were negligible. The test section of the road used was relatively straight. Because of these conditions, it is possible to also assume the dust transport was relatively two-dimensional. From the array of equipment data were acquired for five different primary variables, namely concentration, wind speed, wind direction, and temperature. 10 minute averages for all of these variables were calculated as an initial step in analysis.

Description of Analysis

Means of the primary variables were calculated using Eq. 1,

$$c_a = \frac{1}{t_f - t_i}\int_{ti}^{t_f} c(t)dt \qquad (1)$$

Where

c_a Time average of the variable

$c(t)$ Instantaneous value of the variable

t_f Final time of averaging period

t_i Initial time of averaging period

In the case of this experiment, $t_f - t_i = 10\ min.$ A discrete version of this integral is used as described in Chapra and Canale (2002). Averages and standard deviations for each of the three experiments were derived from these 10-minute averages. Many steps of the analysis to follow require continuous profiles. Due to the discrete nature of the equipment array, assumptions and least square regressions are needed to complete the analysis.

Due to the hillside nature of the site a planar rotation was needed to adequately analyze the wind data. A thorough treatment is given in Wilczak et al. (2001). In addition a number of meteorological quantities of interest were calculated following Stull (1988).

First, the interpolation of vertical wind speed was accomplished by using a logarithmic curve of the form below.

$$u(z) = \frac{u_*}{\kappa}\left[\ln\left(\frac{z}{z_o}\right) - \psi\left(z/L\right)\right] \qquad (2)$$

Where

K Von Karman constant
u_* Friction velocity (m/s)
z_o Aerodynamic roughness length (m)
Ψ Stability function Ψ = - 4.7(z/L) (stable conditions)
L Monin-Obukhov length scale (m); $L = \dfrac{-u_*^3}{\kappa\left(\dfrac{g}{T}\right)\overline{w'T'}}$
T mean temperature measure with sonic the anemometer (K)

$\overline{w'T'}$ Kinematic heat flux (m-K/s)

Additional information on this profile is included in (Arya 2001).

To approximate the vertical concentration profiles, an exponential fit was used as in Veranth et al. (2003). The physical basis and success of Veranth et al. (2003) was the reason this interpolation was used. This profile is defined by the equation below:

$$c(z) = A * \exp(-B * z)$$

Where

$c(z)$ The concentration at a given height

z The height above the ground

A Fitting Parameter

B Fitting Parameter

A least squares reduction may be used to obtain values for the fitting parameters. These reductions are based upon the 10 minute averaged data.

During the majority of the experiment the height of the cloud was consistently located above the highest Dustrak which was located at 5 m. To estimate the top of the cloud a Gaussian Plume model was used.

Gaussian Plume Modeling

Gaussian Plume Models are used to model pollution dispersion. A thorough treatment and derivation is found in Seinfeld and Pandis (1998). Two forms or the equation exist for near ground transport. One assumes the ground is a perfect absorber and the other assumes it is a perfect reflector. For the purposes of the experiment both models give results that differ less than the experimental variability by more than order of magnitude. The model for a continuous plume is given by Eq. 3 below

$$c(x,y,z) = \frac{q}{2\pi U \sigma_y \sigma_z} \exp\left(-\frac{y^2}{2\sigma_y^2}\right) * \left(\exp\left(-\frac{(z-h)^2}{2\sigma_z^2}\right) \pm \exp\left(-\frac{(z+h)^2}{2\sigma_z^2}\right)\right) \quad (3)$$

Where

q Source strength g/s

σ_y Standard deviation relating concentration and position in span wise direction

σ_z Standard deviation relating concentration and position in vertical direction
h Elevation of pollution source.
U Mean Wind speed

The "+" is for the perfect reflector assumption. The "–"is for the perfect absorber. The previous equation is developed for use with a point source. For the purposes of this experiment a relation to a line source is needed. Replacing q *with* an equivalent point source $q' = q/dy$ (i.e. the source strength per unit road length) and integrating over ∞ to - ∞ and using an integration table yields:

$$c(x, y, z) = \frac{2q'}{\sqrt{2\pi} U \sigma_z} \left(\exp\left(-\frac{(z-h)^2}{2\sigma_z^2} \right) \pm \exp\left(-\frac{(z+h)^2}{2\sigma_z^2} \right) \right) \quad (4)$$

Values for different σ_z are available in such sources as the Turner Chart (Turner, 1970), DeNevers (1995), and the EPA (ISC3 1995). Initial analysis of wind data revealed that the Pasquill Stability Categories of D for the no fence experiment and E for the 1 m and 2 m fence experiments. Initial analysis of dust data revealed that a reasonable ambient concentration was 0.015 mg/m^3. To estimate the rate of decay of dust concentration with respect to increasing elevation a least square fit was implemented with the ambient concentration used at elevation of 2.5 standard deviations as an addition data point and using the exponential function as a fitting equation. A perturbation method was used to test sensitivity to the heights assumed. It found the results changed little with reasonable changes to the input heights. Also a corrected distance was used to calculate σ_z . A corrected distance was needed because the mean wind rarely flowed perfectly perpendicular to the road. Thus, the distance traveled by the dust was greater than the downwind distances listed in Table 2. This allows for additional dispersion in the vertical. The corrected length was defined as below:

$$X_c = \frac{X}{Cos(\theta)}$$

Where

X Measured downwind distance from road
X_c Distance traveled by dust
Θ Angle between mean wind distance and line connecting Dustrak towers

To calculate that net horizontal flux of PM_{10} the following equation was implemented with the fitted concentration and wind profiles:

$$Flux = \int_0^T \int_0^\infty c(z,t) * u(z,t) dz dt$$

Where

$c(z,t)$ The dust concentration profile as a function of height above ground
$u(z,t)$ The mean horizontal wind as a function of height above ground
t Time for dust cloud to pass a set point

The integration of the integral utilized a Simpson routine described in Chapra and Canale (2002).

The Gaussian distribution was also used to compare all three experiments to the Gaussian distribution corresponding to the correct Pasquill Stability Category. To estimate the source strength *q'*, in the experimental results data from the roadside Dustraks was implemented in the following equation.

$$q' = UCH_d$$

Where

U The average mean wind from the logarithmic profile. It is averaged between the height z = 2m and the ground
C The average of the concentrations from the two roadside Dustraks
H_d The height of the initial dust cloud

To describe the Gaussian results a relative difference formula is used:

$$Gre = \frac{C_g - C_e}{C_g} * 100$$

Where

C_g Pseudo concentration (C / q') predicted by Gaussian Model
C_e Experimentally measured Pseudo concentration (*C/q'*)

The Gre variable can be informative. A high positive value indicates that the Gaussian model over predicts concentrations. A negative value indicates the opposite. When there is no statistically significant difference in the Gre variable between the three experiments, the effectiveness of windbreaks on dust deposition is either non existent or non determinable using the given data. If a fence experiment has a high Gre compared to the control, no fence, experiment this would indicate that the given fence configuration is effective at dust removal at the given sensor location.

Dispersion Modeling

Eulerian transport models, which balance flow in and out of stationary grid cells, and Lagrangian models, which track the movement of individual particles or fluid packets, are more general than the Gaussian dispersion model. Because of the complexity and computational time associated with Lagrangian models the computational model implemented in this study utilized numerical solutions for an Eulerian atmospheric diffusion equation (ADE). An ADE is derived from a mass balance on a control volume (CV), where species (gases or small particles) are allowed to diffuse in and out of the CV by the turbulent motions of the atmosphere, move through the CV by advection, and are generated from chemical sources and removed by deposition (Seinfeld and Pandis, 1998). ADE models are now relatively common in air quality work. A Gaussian model is a special case of an ADE obtained by assuming flows with homogeneous turbulence along with steady uniform winds. However, wind speed and turbulence in the atmospheric surface layer, have large vertical gradients and do not always satisfy the above simplifying assumptions of the Gaussian model.

The results section will present principally how an artificial canopies height and depth affect the amount of dust transported downwind.

PROBLEMS/ISSUES ENCOUNTERED

Problems encountered during this project include but are not limited to: equipment breakdowns, unpredictability of weather and theft of equipment. Transport of large equipment over hundreds of miles also presented a challenge. Working in an arid environment high in dust concentration was also difficult. Power lines made use of a tethered balloon for measuring dust and wind at greater heights impossible. Air quality effects on the researchers including, runny nose and tearing were symptoms suffered by all of the authors after being present at the test site for only minutes. This arid dusty environment is not ideal for the equipment and increased its maintenance needs. The Authors consider these issues normal to a project of this scope.

A challenge new to the authors was a result of crossing an international border to conduct an experiment. Obtaining the proper permissions for a temporary importation, long delays at the border (on the order of hours), and creation of Mexican collaboration were some new challenges. The Authors strongly feel that the value of performing field research on the

Mexican side of the border greatly out weighs the costs and encourage others to do so. However, we recommend making border transport plans beginning at least six months prior to field work.

RESEARCH FINDINGS

Experiment Results

The atmospheric conditions during the Nogales Sonora experiment are shown in Figures 3 through 8 and displayed in Table 3. Table 3 contains seven variables averaged for each of the four experiments. The first three variables are mean wind speed at different elevations above the ground. The fourth variable is the Monin-Obukhov length scale, L. The roughness height, z_o, the friction velocity (u_*) and wind direction. The table illustrates, that as expected, wind speed increases with elevation in a near logarithmic manner as shown in the table. The results indicate a high amount of shear near the ground. This is indicated by the relatively high value of u_*. Also the wind speed is the highest for the non fence case and is significantly lower for the 1 m and 2 m experiments. Winds were principally from the southwest. The Monin-Obukhov length scale indicates near-neutral to slightly stable atmospheric conditions during most of the experiments.

The mean wind speed, measured at z=5.0 m is shown in Figure 3. The wind velocity is consistently the highest for the no fence experiment, lower for the 1 m fence experiment and lowest for the 2 m fence experiment. The speed is generally steady in all three experiments but decreases as time passes. Figure 4 indicates that for all three experiments the wind direction was predominantly from the south west and was relatively steady. However near the end of the 2 m experiment a change in wind direction to less than 210° invalidated 20 minutes of data. When the flow was so far south of west dust was transported past the south end of the fence. This enabled dust to reach the Dustraks without traveling over or through the fence. This is the reason the plots for the 2 m case end at forty minutes.

In Figure 5 the gradual decay of turbulent kinetic energy is plotted. The decay from unstable conditions to neutral conditions is evident. The magnitude of TKE is relatively unsteady. For the example in the 1 m experiment there is a short period of relatively high TKE indicating a burst of more intense turbulence at about the forty minute point of the experiment.

Figures 6 and 7 display the same unsteadiness of two other turbulence quantities kinematic shear stress, or u_* and sensible heat flux. Both are vary, but are slowly decaying towards more stable values. During the start of the no fence experiment, small positive values of heat flux are measured. Positive values of kinematic sensible heat flux generally indicate an unstable boundary layer. However the small magnitude of the heat flux indicates a near neutral boundary layer. The values during the majority of the experiment, namely moderate values for u_* and small negative values for kinematic heat flux are also indicative of a neutral boundary layer.

Figure 8 confirms the previous conclusions. The Monin-Obukhov length scale, L, is a measure of buoyancy driven turbulence in the atmosphere. The large positive values indicate an atmosphere with negligible buoyancy generated turbulence. At the start of the no fence example, the L scale is negative, which generally indicates a unstable atmosphere. However the magnitude is so large that this length scale indicates a stable boundary layer. This parallels the heat flux conclusion for the no fence experiment in Figure 7 because the Monin-Obukhov length is a function of kinematic shear stress.

Figure 9 illustrates the decay of mean concentration with downwind distance. In Figure 9 the local concentration, C is divided by the road side concentration Cr. The figure suggests the decay is of an exponential form. This is consistent with data from previous studies. Figure 9 displays this decay for all three experiments at z = 2 m. Similar plots for different elevations would display similar trends.

Figure 10 shows the same data but in bar charts with the concentration standard deviation indicated. Normalized concentrations are displayed at x = 46.8, 23.7, and 0.9 m downstream of the road for the elevation z=2 m. As in Figure 9, Figure 10 displays an exponential type of decay. It also illustrates an additional point, as downwind distance increases the spread in the data, as indicated by error bars, increases when compared to the normalized concentrations. The data variability increases as dust diffuses outward. The increase with spread of distance is common to most results in this study.

Figure 11 shows the comparison of the concentration data to the Gaussian plume model. Two points, both at z= 2 m and one at x = 46.8 the other at x = 23. 7 m downwind were used as comparison points. The basis for the use of the three points was that at other points the Gaussian model poorly described the experimental concentration field. Other points were either too close to the road or ground. Also compared to the data from the x= 23.7 m z= 5 m Dustrak, the Gaussian solution placed an excessive fraction of the distribution of the dust under the z =5 m Dustrak. Because of this the point is not included in the plots.

On the left-hand side of Figure 11, the sensor located at x =23. 7 m and z = 2 m indicates a slight statistical difference between the three configurations. The no fence and 1 m fence results are similar with a small indication that the 1 m fence configuration may be somewhat effective at lowering dust concentrations. The 2 m fence displays an even higher distribution of values for *Gre*. The higher distributions suggest that the 2 m fence is effective at lowering concentrations at this distance. The right-hand plot provides the same conclusion for the downwind distance x= 46.8 m, but has a much more significant difference for the 2 m configuration. The difference between no fence and the 1 m meter configurations at this distance are virtually indistinguishable.

Figure 12 displays the mean results from the dust flux method. It displays the mean fraction of dust advected down wind *Fs* compared to the mass initially suspended *Fo.* It indicates that directly behind the fence, the amount of dust advected downwind is actually increased by the presence of the fence directly behind the fence. The increase in dust flux is most acute for the 2m configuration. It is most likely due to the decrease in high momentum airflow behind the fence. This slow flow, or possibly backflow, creates an increase in residence time for a given particle of dust in this area. This increase in residence time leads to higher concentrations. These higher concentrations yield higher fluxes of dust. The flux of dust quickly decreases downwind for all three experiments. However the data tends to indicate that the taller the fence the greater the rate of decrease of flux with down wind distance. At distances of about 50 m the 2 m flux has decreased to a value less than the no fence and 1 m experiments. This is mostly likely also due to the increased residence time behind the fence. The increased residence time also promotes enhanced deposition, and hence lower fluxes at distances of the order of 50 m.

The distribution information on the 10 min averaged data for fluxes is shown in Figure 13. This figure does not display the increase in the spread of data with increasing downwind distance. Based on the flux method the data indicates that an artificial ski fence can be effective at reducing dust fluxes at distances on the order of 50 m. It seems to indicate that directly behind the fence the flux of dust is increased. At middle distances, about 25 m, the data indicates that for this experiment artificial windbreak effectiveness is indeterminate.

The ADE computational model was used to test the indication that canopy would be an important variable in building an artificial windbreak as a dust control strategy. This model assumes a deep fetch unlike the experiment. Despite this difference, some additional insights may be gained for artificial fetches. Figure 14 is from Pardyjak et al. (2007). *H** is a ratio of canopy height to initial dust cloud height. Figure 14 indicates that the ratio of canopy height to initial dust cloud height is an extremely important parameter. Rapid decreases in emitted dust are observed with increasing canopy height given the same height for an initial dust cloud. This height effect seems to dominate even stability effects. Details of the simulation are given in Appendix 1.

Figure 15 indicates that the rate of dust redeposition is initially high, but decreases in an exponential manner with increasing downwind distance. This seems to indicate that an increase in canopy or windbreak height is more effective than increasing fetch depth in decreasing fugitive dust emissions from roads.

CONCLUSIONS

The Nogales Sonora data together with the simulation data suggest that artificial windbreaks may be used as an effective dust control plan, however much more work should be done to identify the importance of different geometric and atmospheric parameters on deposition.

The field experiments indicate that strong downwash flow associated with taller fences may lead to enhanced deposition, while shorter fences showed little or no effectiveness.

The combined simulation and experimental results indicate that for a given type of mitigation effort, an increase in canopy height is more effective than adding multiple rows of artificial windbreaks. The computational calculations also indicate that this conclusion is valid for different atmospheric stabilities. This is encouraging given the typical limited economic and spatial resources available.

RECOMMENDATIONS FOR FURTHER RESEARCH

As in all experimental studies, additional data is necessary. Experiments at different sites and under different meteorological conditions would increase our general understanding of artificial windbreaks. Specifically, a more systematic set of experiments that vary upstream roughness, windbreak porosity, atmospheric stability as well as the “character of the snow fence” (i.e., the type of material, shape of pores, etc). Also, a more realistic model of the momentum deficient air flow behind the artificial wind break is necessary for evaluating different windbreak strategies. The current ADE model can predict momentum deficits given on a few parameters dependent upon the windbreak, but does not correctly model recirculating flows for dense windbreaks. Additionally, an improvement in dry particle deposition model is needed for different types of depositing surfaces and particles. To date, there are many models but their predictions for dust deposition under a given set of parameters may vary over an order of magnitude.

RESEARCH BENEFITS

SCERP and other researches have thoroughly documented the high concentrations of Particulate Matter due to fugitive dust emissions in which border residences live and work (Zaragoza 2002) (Border 2012 Ambos Nogales Air Quality task force 1995). Practical approaches that reduce particulates will improve health and prolong lifespan. Quality of life is also enhanced. Policy makers can utilize tools and studies such as those discussed in this work to reduce particulate concentrations. The more practical the approach, the more likely it is to be implemented. The computer simulation is described in two peer reviewed journal articles currently under review and are included as Appendices.

Also, a collaboration with the faculty and students of the Nogales Campus has been created. During the months of July and August 2006 two students, Diana Ruth Felix Chavez and Rito Duarte Dominguez, along with a teacher, Fernanda Villalobos Robles visited the University of Utah campus. After speaking with various SCERP funding researchers, such as Shane Cutler and Bonnie Tyler, Diana and Rito produced an informative presentation on the Air Quality issues facing the quickly growing Nogales area. As part of the presentation practical suggestions were offered by Diana and Rito.

ACKNOWLEDGMENTS

The authors are indebted to Diane Austin of the University of Arizona for her help in establishing contact with the administration of CONALEP. Rosalva Leprón de León of CONALEP spent hours with the authors at the border and was available for assistance multiple times. The complete faculty of CONALEP provided more assistance than was reasonable to ask. Alma Cota of Fundación del Empresariado Sonorense (FESAC) also provided vital assistance with importation of equipment.

This work was sponsored by the Southwest Consortium for Environmental Research and Policy (SCERP) through a Cooperative agreement with the U.S. Environmental Protection Agency. SCERP can be contacted for further information through

www.scerp.org and scerp@mail.sdsu.edu

REFERENCES

Arya, S. P., (2001). Introduction to Micrometeorology, 2nd Edition, Academic Press.

Border 2012 Ambos Nogales Air Quality task force, Border Liaison Mechanism Economic and Social Development Subgroup. (2005) Plan of Action for improving air quality in Ambos Nogales

Chapra, S.C. and Canale, R.P., (2002). Numerical Methods for Engineers, 4th edition. Mc GrawHill.

Cionco, R. M., (1965). Mathematical model for air flow in a vegetative canopy. J. Applied. Meteorol.*,* 4**,** 517-522.

De Nevers, N. (1995). Air pollution control engineering. New York, McGraw-Hill.

EPA (1995). Users Guide for the Industrial Source Complex Dispersion Models. Office of Air Quality Planning and Standards Emissions, Monitoring, and Analysis Division Research Triangle Park, North Carolina

Etyemezian, V., S. Ahonen, D. Nikolic, J. Gilles, H. Kuhns, D. Gillette, and J. Veranth (2004). Deposition and Removal of Fugitive Dust in the Arid Southwestern United States: Measurements and Model Results. Journal of the Air and Waste Management Association 54: 1099 – 1111.

McNaughton, K.G. (1988) Effects of Windbreaks on Turbulent Transport and Microclimate. Agriculture, Ecosystems and Environment 22/23: 17-39.

Pardyjak E. R., Speckart S., Yin F., and Veranth J. M. Near Source Deposition of Vehicle Generated Fugitive Dust on Vegetation and Buildings. Part 1: Model Development and Theory, submitted to Atmos. Environ. October 2007.

Pardyjak E. R. and Speckart S. (2006) Assessment of Windbreaks as a Dust Control Strategy for communities in arid climates such as the US-Mexico border region SCERP project number A-04-03

Samet, J.M., Zerer, S.L., et al. (1998). Particulate Air Pollution and Mortality: The Particle Epidemiology Evaluation Project. Applied Occupational and Environmental Health 13(6): 364-369.

Seinfeld, J.H. and Pandis, S.N. (1998). Atmospheric Chemistry and Physics — From Air Pollution to Climate Change. New York, Wiley.

Stull R. (1998) An Introduction to Boundary Layer Meteorology. Kluwer Academic Publishers

Turner, D. B. (1970). Workbook of atmospheric dispersion estimates. Washington, U.S. Government Printing Office.

Wilczak, J. M., Oncley, S. P., and Sage, S. A. (2001). Sonic Anemometer Tilt Correction Algorithms, Boundary-Layer Meteorol. 99, 127–150.

Veranth, J. M., Seshadri, G. and Pardyjak, E. (2003). Vehicle-generated fugitive dust transport: Analytic models and field study. Atmospheric Environment 37(16): 2295-2303.

Veranth, J. M., Speckart S., Yin F., Etyemezian V. and Pardyjak, E. Near-source deposition of Vehicle-Generated Fugitive Dust on Vegetation and Buildings. Part 2. Field Measurements and Model Validation. Submitted to Atmos. Environ. October 2007.

Zaragoza, Xavier (2002) “It’s all up in the air.” The Daily Dispatch (April 27-28)

Table 1. Experimental times for the experiments conducted on CONALEP campus in Nogales, Sonora during May 2006.

No.	Experiment	Start Time(MST)	End Time(MST)	Traffic (cars/hour)
1	No Fence	18:00	19:00	200/hr
2	1 m Fence	19:30	20:30	270/hr
3	2 m Fence	19:30	20:10	190/hr

Table 2. Experimental layout x=distance downwind of road (m) z=elevation aboveground (m).

Equipment	X	Z
Dustrak	0.5	0.5
Dustrak	0.5	2
Dustrak	0.9	0.5
Dustrak	0.9	2
Dustrak	23.7	2
Dustrak	23.7	5
Dustrak	46.8	0.5
Dustrak	46.8	2
Sonic	23	1.37
Sonic	23	2.93
Sonic	23	5

Table 3. Summary of Averaged variables for Experiments 1 through 3. Note that WS/WS(5m) is the wind speed normalized by the speed at 5 m.

Experiment	1	2	3
Wind Speed z=1.37 m	3.07	1.96	1.23
Wind Speed z=2.93 m	3.69	2.10	1.43
Wind Speed z=5.0 m	4.10	2.25	1.56
WS/WS(5m) z = 1.37 m	0.75	0.87	0.79
WS/WS(5m) z = 2.93 m	0.90	0.93	0.92
WS/WS(5m) z = 5.0 m	1	1	1
L (m)	416.1	428.8	125
z_o (m)	0.0257	0.0198	0.0144
u_* (m/s)	0.429	0.403	0.248
Direction (degrees)	252	226	240
Stability Class	D	E	E

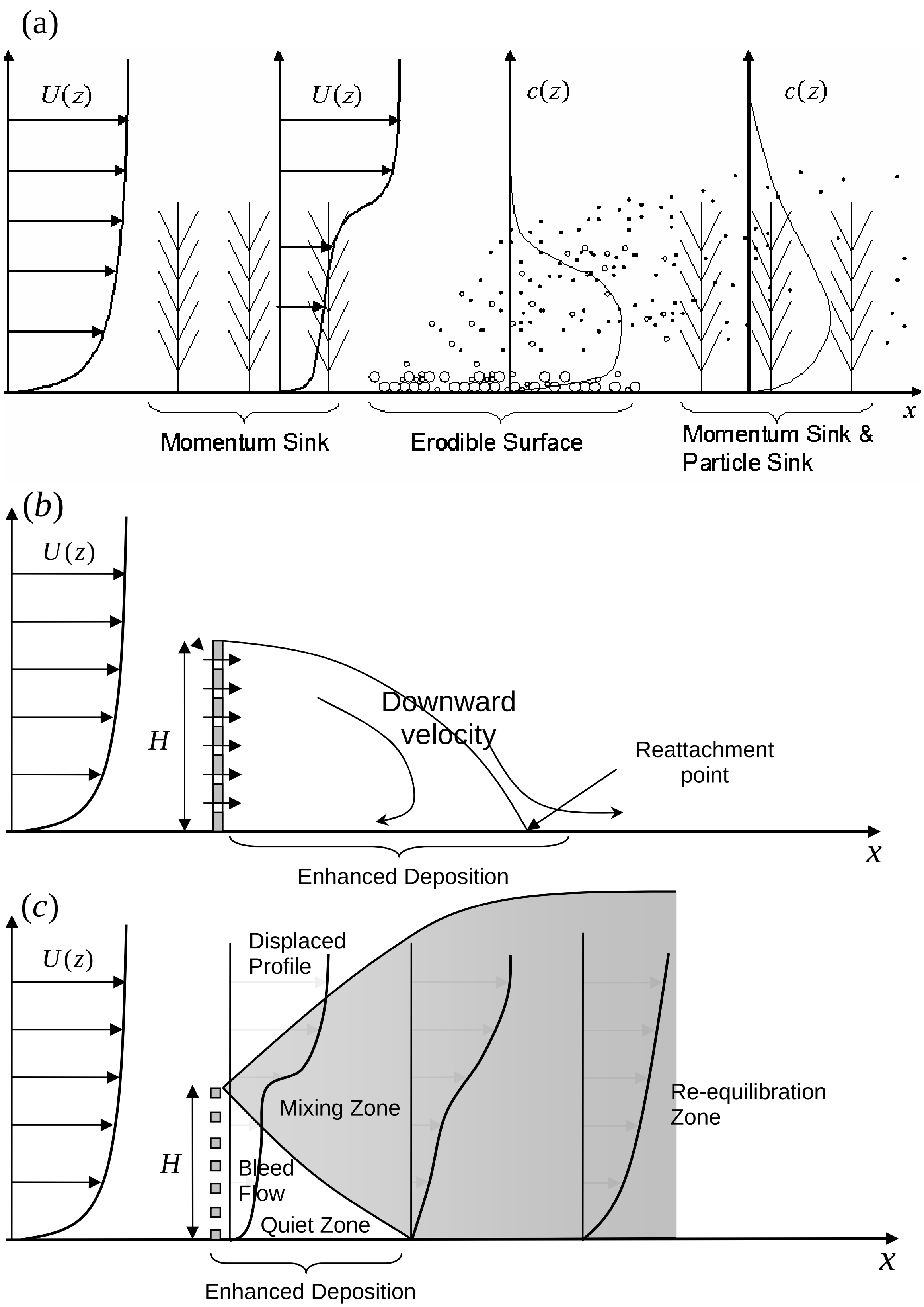

Figure 1. Physics of Dust Removal from (a) deep vegetative canopy, (b) high solidity windbreak and (c) low-solidity wind break.

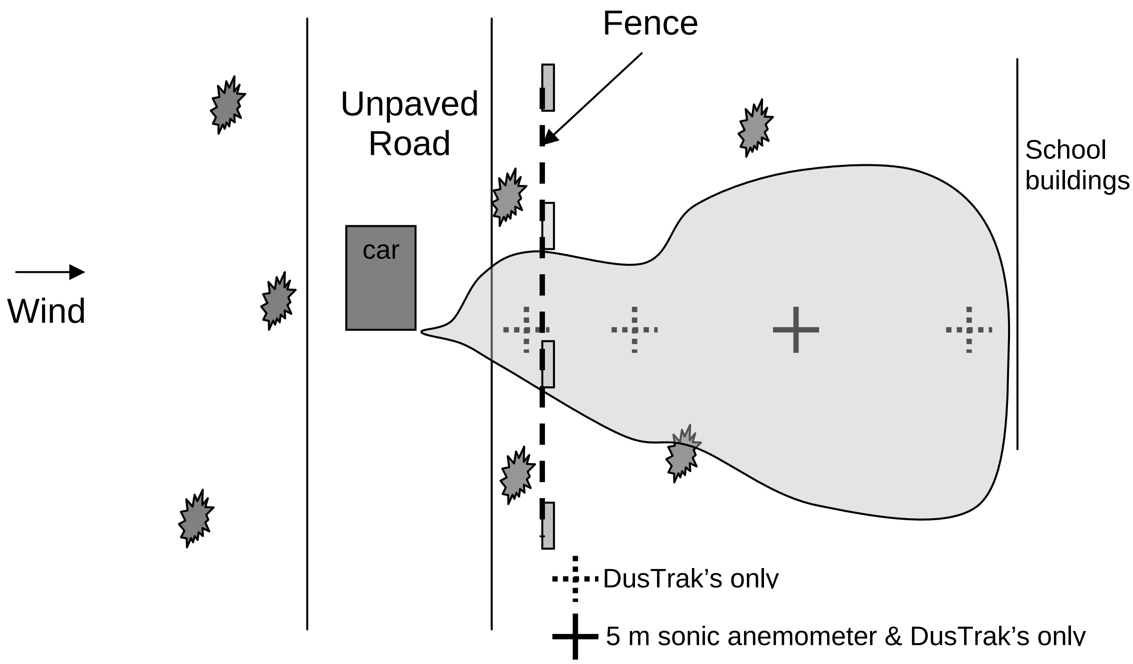

Figure 2. Schematic of the fugitive road dust experimental setup in Nogales, Sonora at CONALEP.

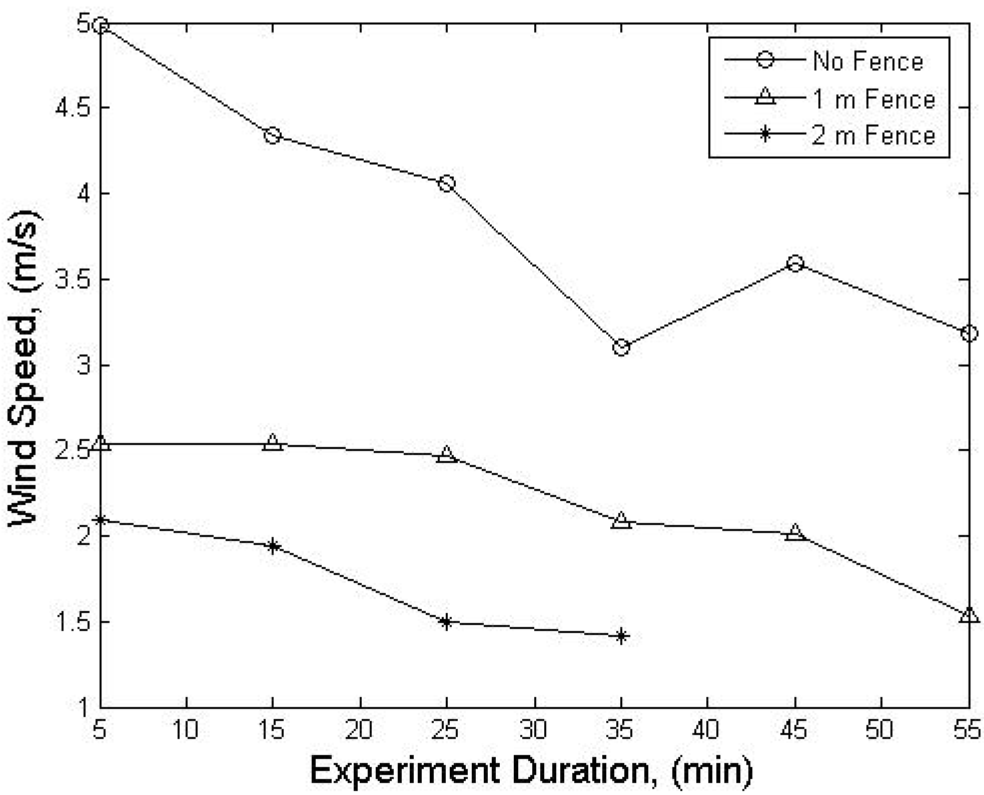

Figure 3. Mean (10 minute averaged) wind speeds during the three experiments conducted on May 25, 28, and 29th 2006.

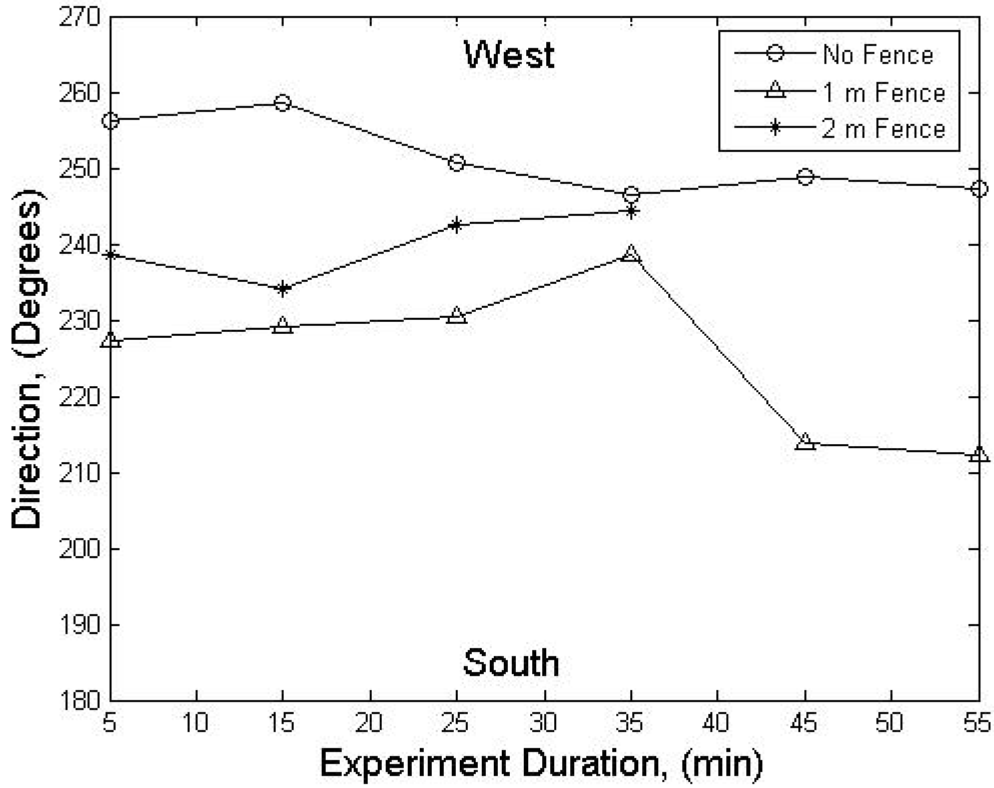

Figure 4. Mean (10 minute average) wind directions during the three experiments conducted on May 25, 28, and 29th 2006.

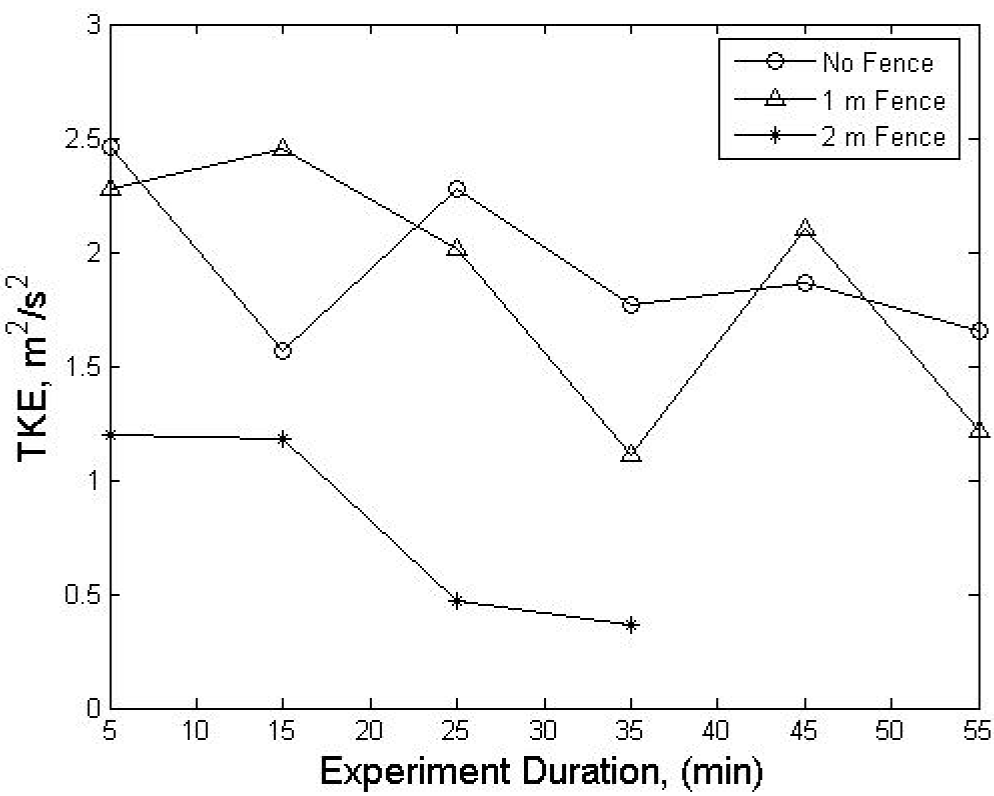

Figure 5. Slight Decay of turbulent kinetic energy (TKE, 10 minute averages) during the three experiments conducted on May 25, 28, and 29th 2006.

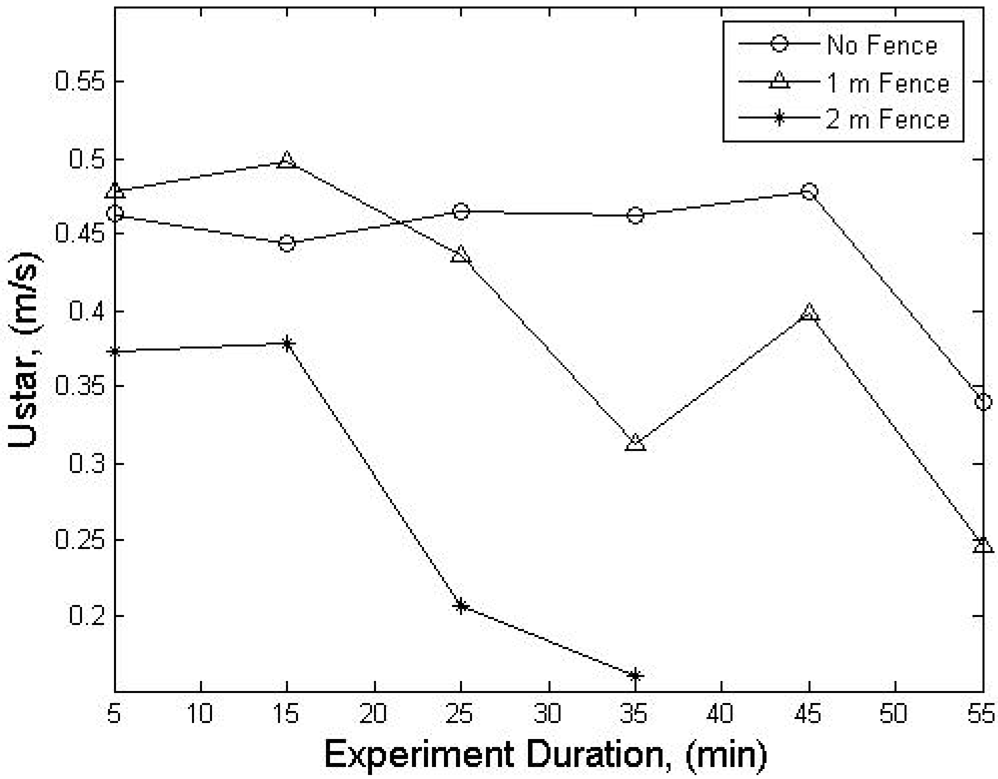

Figure 6. Slight Decay of kinematic shear stress, ustar (10 minute averages) during the three experiments conducted on May 25, 28, and 29th 2006.

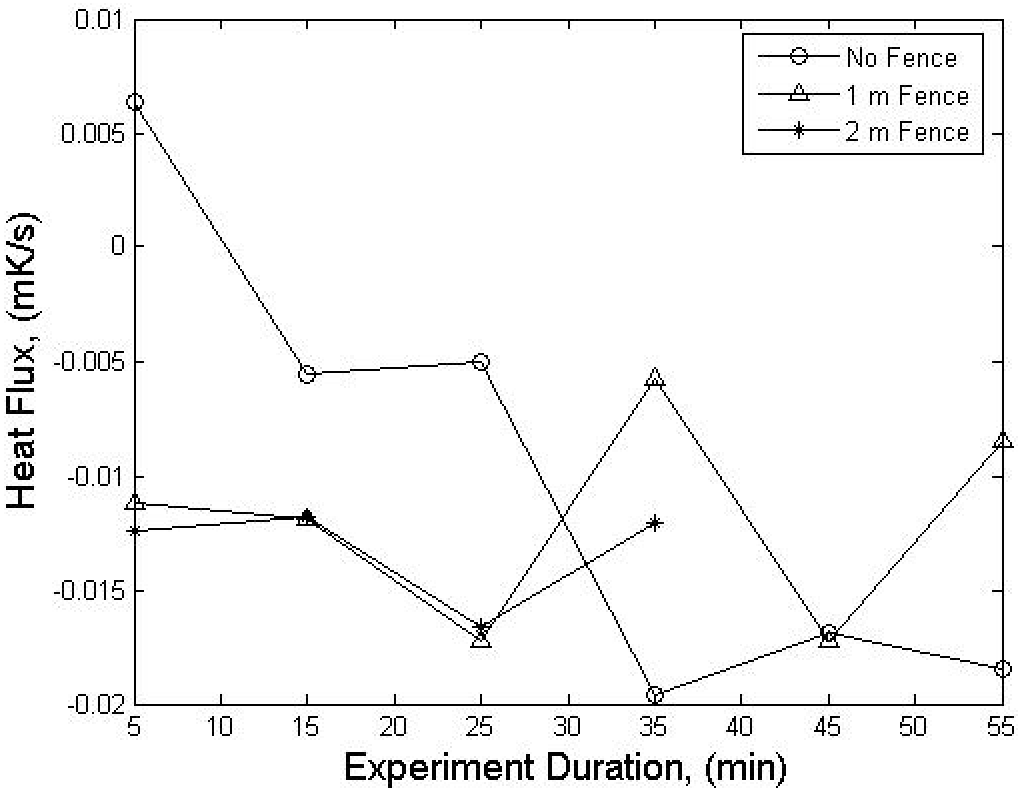

Figure 7. Gradual Transition of kinematic sensible Heat Flux (10 minute averages) during the three experiments conducted on May 25, 28, and 29th 2006.

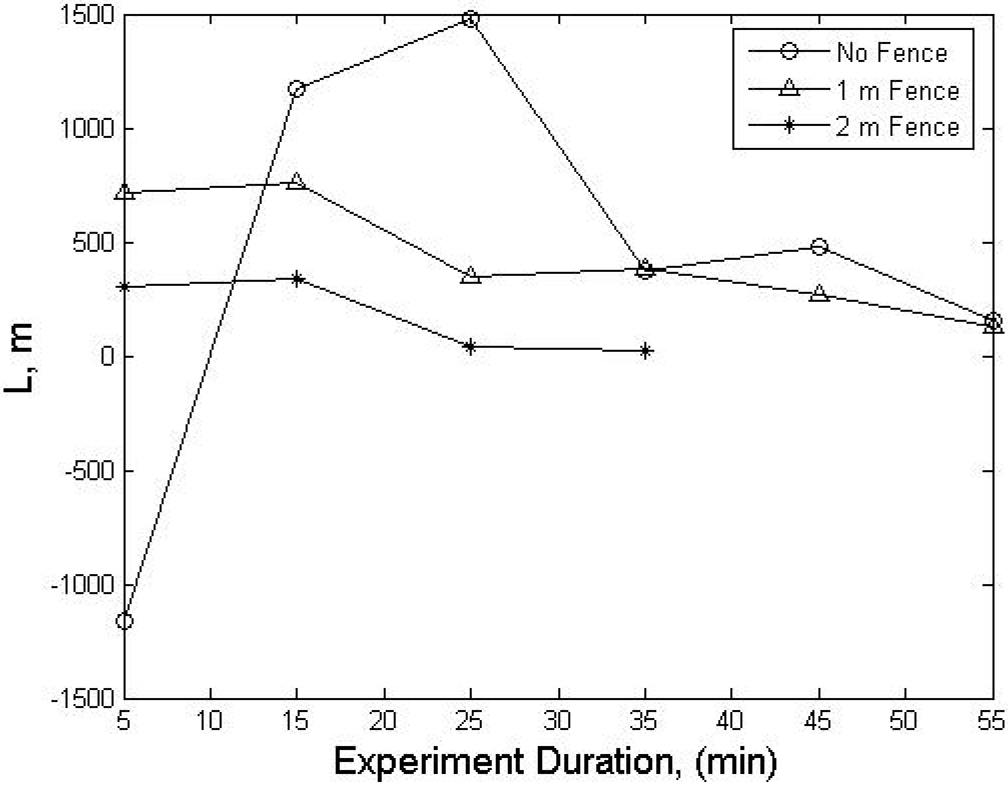

Figure 8. Monin-Obukhov Length Scale, L, (10 minute averages) during the four experiments conducted on May 25, 28, and 29th 2006.

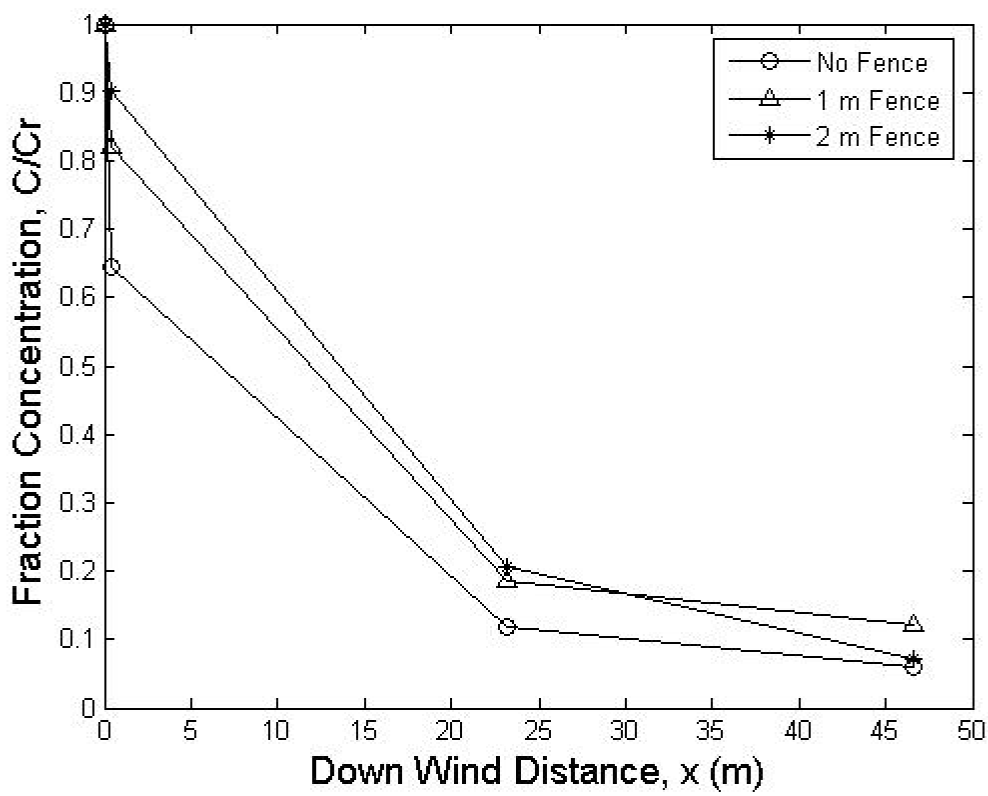

Figure 9. Decrease of mean Concentration with downwind distance at z = 2 m.

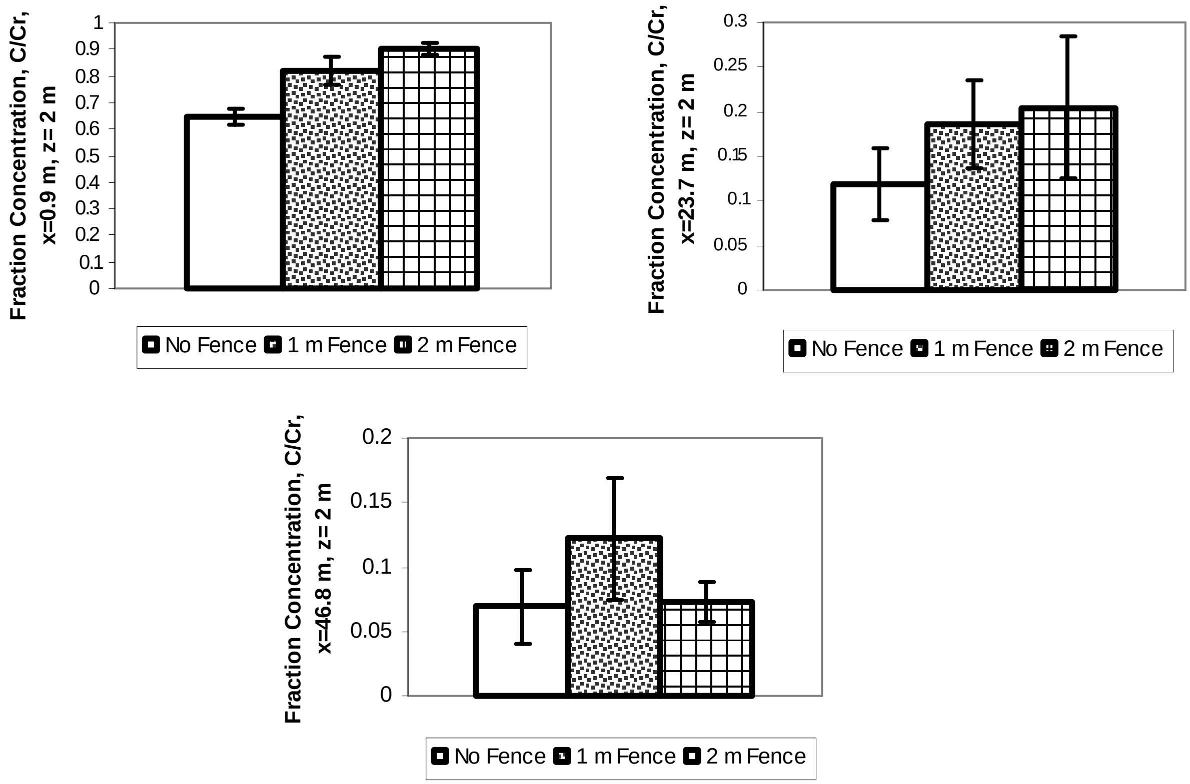

Figure 10. Statistical distribution of decrease in normalized concentration downstream of the unpaved road. All three experiments

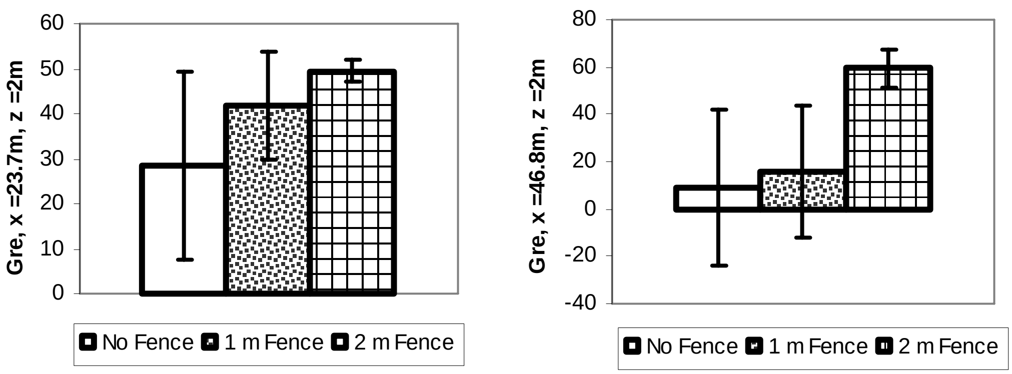

Figure 11. Comparison between Gaussian Plume model and experimental results. *Gre* is percent relative difference between the Gaussian model and experimental results

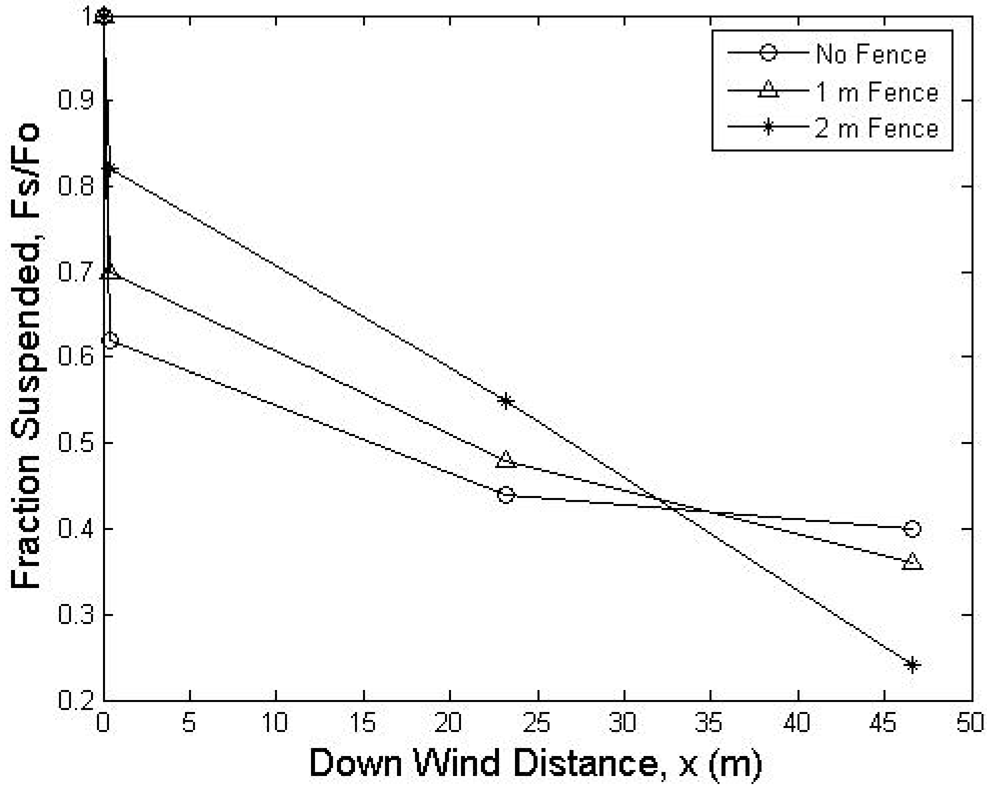

Figure 12. Downwind decay of mean horizontal flux of dust with downwind distance.

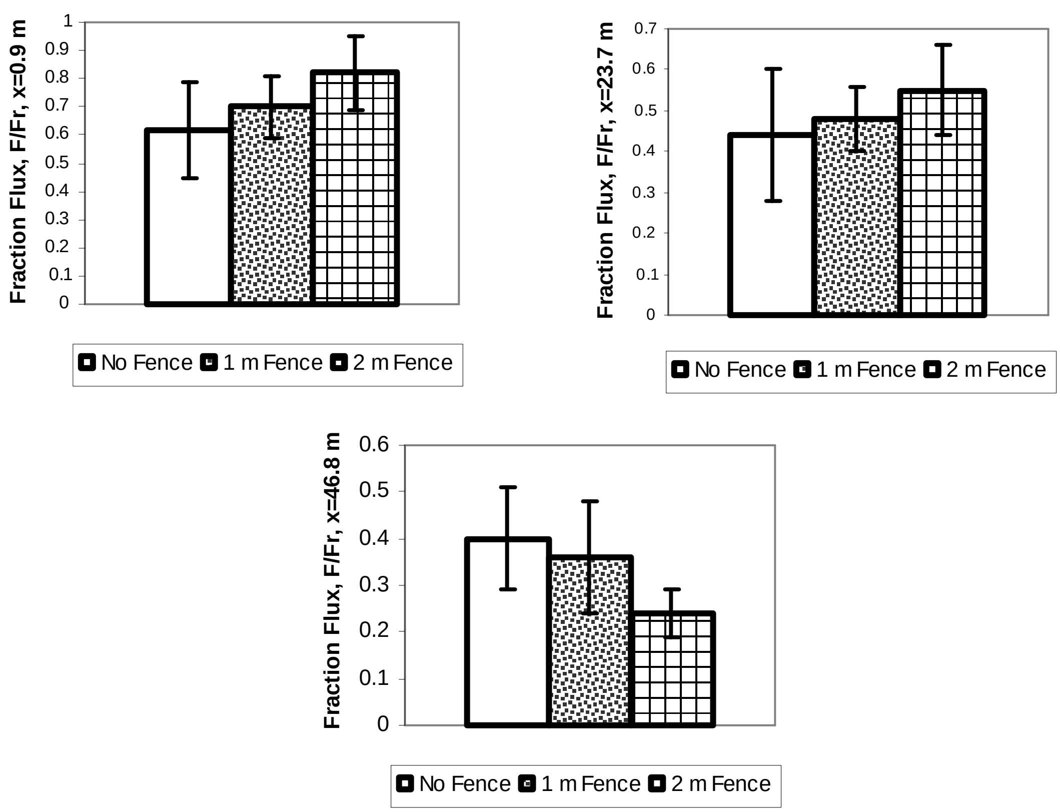

Figure 13. Distributions of downwind reduction of dust flux at x = 0.9, 23.7 and 46.8 m down stream.

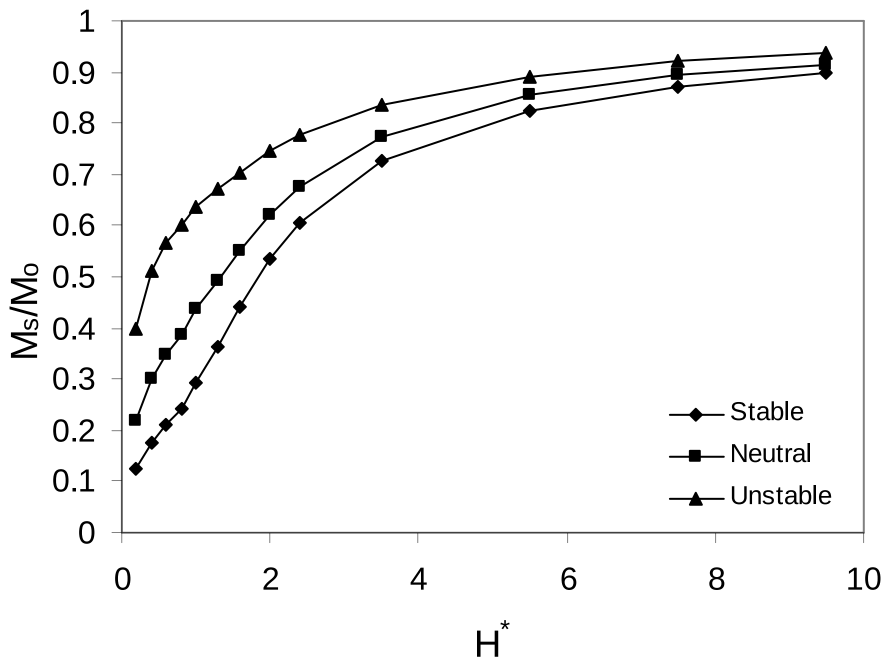

Figure 14. Simulation result displaying the effects of the ratio of canopy height to initial dust cloud height H* to total mass suspended to initial dust suspended. Ms/Mo

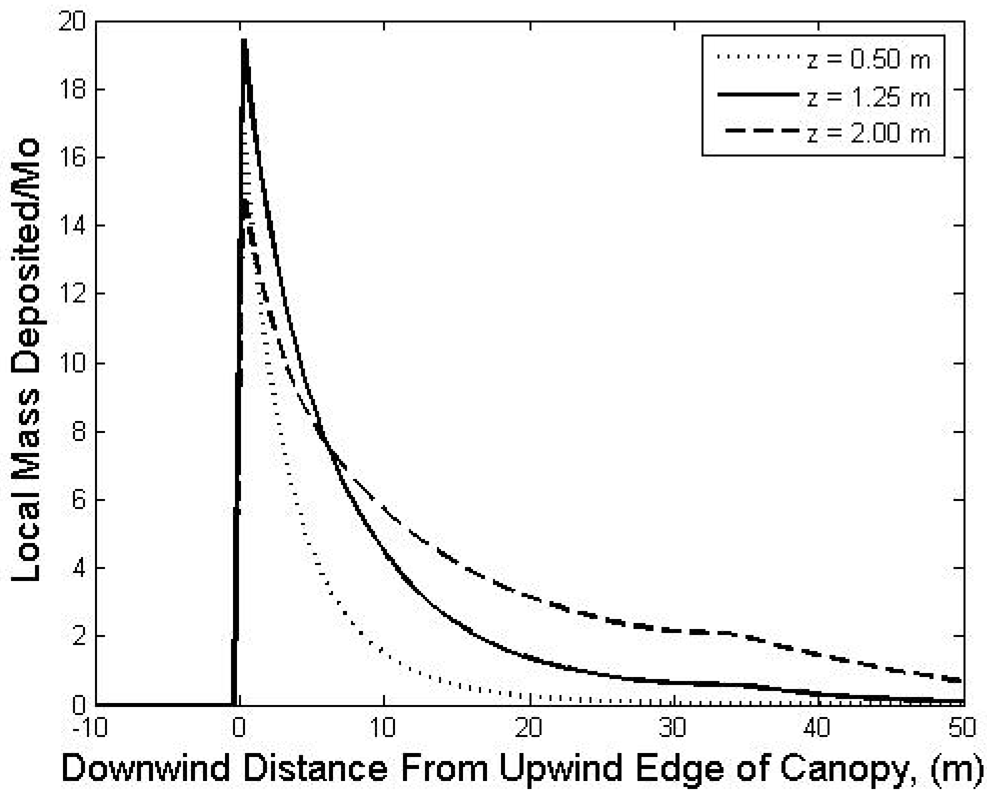

Figure 15. Simulation result displaying the decrease in local mass deposited per unit mass suspended with downwind distance.

APPENDIX 1

Near Source Deposition of Vehicle Generated Fugitive Dust on Vegetation and Buildings, Part I: Model Development and Theory

E.R. Pardyjak[1], S.O. Speckart[1], F. Yin[2] and J. M. Veranth[3]

1. Department of Mechanical Engineering, University of Utah, Salt Lake City, Utah

2. Department of Chemical Engineering, University of Utah, Salt Lake City, Utah

3. Department of Pharmacology and Toxicology, University of Utah, Salt Lake City, Utah

Manuscript for submission to
Atmospheric Environment

October 17, 2007

Corresponding Author
Eric R. Pardyjak
University of Utah
Room 2110
Salt Lake City, UT 84112
Tel: 801-585-6414 Fax: 801-585-0039
pardyjak@eng.utah.edu

Abstract

This paper describes the development of a simple quasi-2D Eulerian atmospheric dispersion model that accounts for dry deposition of fugitive dust onto vegetation and buildings. The focus of this work is on the effects of atmospheric surface layer parameterizations on deposition in the “impact zone” near unpaved roads where horizontal advection of a dust cloud through roughness is important. A wind model for computing average and turbulent wind fields is presented for flow within and above a roughness canopy. The canopy model has been developed to capture the most essential transport and deposition physics while minimizing the number of difficult to obtain input parameters. The deposition model is based on a bulk sink term in the transport equation that lumps the various dry deposition physical process. Wind field, turbulence and deposition results are presented for a range atmospheric stabilities and roughnesses. The canopy model produces results in which deposition within a canopy is enhanced under certain initial, atmospheric and roughness conditions, while under other conditions much less deposition occurs. The primary limitation of the model is the ability to accurately determine (typically using experimental data) the vegetative deposition parameter (clearance frequency). To understand the clearance frequency better, a dimensionless parameter called the transport effectiveness is identified and the limiting cases discussed. In general, the model captures the essential physics of near source dust transport and provides a tool that can efficiently simulate site-specific conditions in practical situations.

Keywords: fugitive dust; near-source deposition; roughness; vegetation; vehicle generated dust

1. Introduction

Vehicle generated fugitive dust is the uncontrolled emission of particulate matter associated with vehicles driving over unpaved roads. These emissions are particularly important in populated arid regions with many kilometers of unpaved roads such as the cities along the U.S./Mexico border. The amount of fugitive dust that is transported long distances from these sources can have a great impact on health (Davidson et al., 2005) and visibility (Watson and Chow, 1994). A number of abatement strategies exist including the application of liquids onto unpaved roads (Harley et al., 1989) but many options are uneconomical or ineffective in arid climates with extensive rural roads. It has been proposed that another strategy for reducing these emissions is to utilize natural vegetation and windbreaks (Pace, 2005). In addition, studies indicate (Watson and Chow, 2000), that current EPA emission factors over predict long range transport. One hypothesis for this overestimate is that the emission factor model does not account for particle removal by vegetation or other roughness elements near the source. In order to understand the net emissions from unpaved roads, it is necessary to quantify the amount of dust that is deposited near the source before the dust cloud is well mixed.

There have been a wide range of studies focusing on measuring and modeling the dry deposition of particles onto vegetation and other surface roughness (for reviews see e.g., Nicholson, 1988; Sehmel, 1980; Seinfeld and Pandis, 1998). Dry deposition of particles in the atmospheric boundary layer is governed by the turbulent flow characteristics, the physical and chemical properties of the material being deposited and the nature of the surface (Seinfeld and Pandis, 1998). Deposition of particles onto surfaces occurs primarily by the following mechanisms: impaction, Brownian diffusion, interception, gravitational settling (or sedimentation) and phoretic (diffusiophoresis, thermophoresis, electrophoresis) precipitation (Nicholson, 1988).

Impaction and gravitational settling occur when particles cross streamlines as a result of particle inertia. In Brownian diffusion, particles cross streamlines as a result of molecular bombardment of air molecules on particles. Interception occurs when the radius of the particle is large compared to the particles distance to the surface of the intercepting element (e.g. leaf). Much of the existing literature related to particle deposition onto roughness elements (Chamberlain, 1975; Raupach et al., 2001; Slinn, 1982) considers transport far downwind of the source where concentrations are relatively uniform with height and the horizontal surface is considered a sink. This type of problem is typically modeled using a deposition velocity formulation that considers different physical processes as a resistance network analogy (Seinfeld and Pandis, 1998).

Deposition near the source, or more specifically in the "impact zone", however is less well understood. Figure 1 illustrates the limiting cases for dust transport (adapted from Etyemezian et al., 2004) near an unpaved road. The limiting cases include the impact, transition and far downwind zones. In the impact zone, the height of the dust cloud is of the same order of magnitude as the height of the vegetation, terrain irregularities, fences, buildings, or other roughness elements. The concentration of dust is highest near the ground. In the transition zone, the cloud is much taller and vertical concentration gradients are lower compared to the impact zone. In the far downwind zone, the dust is fairly uniformly distributed throughout the height of the atmospheric surface layer, except very near the ground. This study focuses on dust removal very close to the road where the dust cloud is in the impact zone.

Etyemezian et al. (2004) studied the behavior of a dust cloud downwind of a dirt road at Ft. Bliss, near El Paso, Texas U.S.A. during late spring 2002. The test site consisted of small dunes with widely spaced desert shrub vegetation (aerodynamic roughness of ~0.001-0.01 m) and neutral to unstable atmospheric conditions. The field data were compared to a line source Gaussian plume model in a near-road dust simulation. The measurements indicated that the loss of PM_{10} (particulate matter with an aerodynamic diameter of 10μm or less) within 100 m downwind of the source was within measurement uncertainty (less than ~10%). The EPA Industrial Source Code version 3 (ISC3), a Gaussian based model, indicated the loss of PM_{10} to be less than 5%. Etyemezian et al. (2004) concluded that the EPA ISC3 model is a simplistic but reasonable first approximation for this problem.

Veranth et al. (2003) studied a similar dust dispersion problem downstream of a dirt road in Utah's west desert at The U.S. Army Dugway Proving Grounds (DPG). They investigated the loss of PM_{10} through a mock array of buildings downwind of an unpaved road under stable atmospheric conditions. The downstream surface roughness was created using shipping containers (2.5 m high, 2.4 m deep and 12.2 m long) in a rectangular 10 × 12 array. The data revealed a removal of 85% for PM_{10} within the first 100 m downwind. Etyemezian et al. (2004) also used the Gaussian based model to analyze this experiment assuming very stable conditions and a much larger roughness height, (0.71 m) than for the Ft. Bliss study. The Gaussian model predicted only 30% removal for the DPG experiment. We hypothesize that the discrepancy between the Ft. Bliss and DPG data is a result of the Gaussian model's inability (due to the model's basic assumptions being violated) to capture the complex physics associated with flow through buildings capped by a stable inversion. The discrepancy between the two problems has motivated the authors of the present paper to develop a simple model that more accurately captures the physics associated with dust transport through roughness elements subject to different atmospheric stabilities.

In order to develop a practical model for deposition, the wind and turbulence field through the roughness elements must be carefully modeled. In recent years, a great deal of progress has been made regarding understanding turbulent flow through and above obstacles in the atmospheric surface layer. In particular, flows associated with vegetation (Finnigan, 2000; Raupach and Thom, 1981) and buildings (Belcher, 2005; Britter and Hanna, 2003) have received much attention. While the details of the fundamental processes that govern the flow within vegetative and building canopies are quite different, some of the bulk properties can be modeled similarly. For example, the results of (Macdonald, 2000) for mean flow and turbulence parameterizations for groups of buildings, which is based on the vegetative canopy model, yield a good comparison to experimental results. One of the goals of the present work was to build on this previous canopy research to develop a simple model for the mean velocity and turbulence that can be easily applied to fugitive road dust problems in the impact zone. This has been done using a simple two dimensional Eulerian atmospheric diffusion equation model described below. An attempt is made to minimize the number of difficult to obtain input parameters while retaining import physical processes. For example, if the geometry of the problem is known (i.e. height of the canopy, type of canopy, road width, distance from road to the roughness and typical vehicle height) and the deposition coefficient (described in detail in section 2.2) can be estimated, the model can implemented if the upstream wind speed is known at a reference height along with an estimate for atmospheric stability. Other wind (Harman and Finnigan, 2007; Macdonald, 2000; Poggi et al., 2004) and deposition models (Aylor and Flesch, 2001; Raupach et al., 2001; Slinn, 1982) require detailed knowledge of the roughness elements. Below, we present the development of the model and the general performance of the model. In the companion paper (Veranth et al., 2007), the model is validated with full scale experimental data.

2. Methods

2.1. Atmospheric Diffusion Model

Eulerian transport models, which balance flow in and out of stationary grid cells, and Lagrangian models, which track the movement of individual particles are more general than Gaussian dispersion models because they are able to more easily incorporate complex physical processes (Ramaswami et al., 2005; Seinfeld and Pandis, 1998). Because of the complexity and computational time associated with Lagrangian dispersion models, this study utilized numerical solutions to a quasi-two dimensional Eulerian atmospheric diffusion equation (ADE). For this work, an ADE has been derived from a mass balance on a control volume (CV) in which small particles are allowed to transport in and out of the CV by mean advection and turbulent motions of the atmosphere. Molecular diffusion is assumed negligible compared to turbulent diffusion and turbulent diffusion is modeled using *K-Theory*; additionally, source (dust generated by vehicular motion) and sink (deposition) terms may be defined in each cell following Seinfeld and Pandis (1998). ADE models are now relatively common in air quality work. A Gaussian model is a special case of the solution of an ADE obtained for flows with homogeneous turbulence along with steady uniform winds (Seinfeld and Pandis, 1998). However, wind speed and turbulence in the rough wall atmospheric surface layer, have complex gradients that do not always satisfy the simplifying assumptions of the Gaussian model.

The 2D ADE used in this study is modified to consider dust deposition on a rough walled surfaces (e.g., vegetation or buildings) or the ground (flat surface) as shown below in Eq. 1:

$$\underbrace{\frac{\partial c}{\partial t}}_{I} = \underbrace{-\frac{\partial cu}{\partial x}}_{II} \underbrace{+\frac{\partial}{\partial z}\left(K_{zz}\frac{\partial c}{\partial z}\right)}_{III} \underbrace{-\frac{\partial cV_s}{\partial z}}_{IV} \underbrace{-V_d A_V c}_{V} \; . \qquad (1)$$

In Eq. 1, c is the concentration of dust in (mg m^{-3}), u is the local streamwise velocity in m s^{-1}, K_{zz} is the vertical turbulent mixing coefficient in m^2 s^{-1}, V_s is the gravitational settling velocity in m s^{-1}, V_d is the horizontal deposition velocity onto the roughness elements in m-s^{-1} and A_v is the effective deposition area per volume of space m^2 m^{-3} and includes the ground surface. Equation 1 is an ensemble averaged equation; hence c and u are ensemble averaged quantities. The physical interpretation of the terms is as follows: term *I* is the local accumulation of dust within a CV; term *II* is the advection of dust by the mean flow; term *III* represents the turbulent diffusion in the vertical direction; term *IV* is the gravitational setting, and term *V* represents the total practical deposition sink to the vegetation. Term *V* does not explicitly differentiate all of the different mechanisms associated with deposition onto roughness elements, but rather bulks the processes together into one lumped term. As noted above, this is a "quasi" 2D model because the velocity field is specified by a canopy profile model that is described in following sections, not by a set of prognostic equations. While the canopy model described herein does not explicitly resolve the geometry of the vegetation, it does include the effects of the vegetation on the momentum field.

2.2. Deposition model

Specifying the effective deposition area per unit volume A_V can be quite difficult for complex vegetative or anthropogenic surfaces, and the numeric value for V_d depends on the assumptions made regarding the surface area. However the $V_d A_V$ product can be directly obtained from measurements of mass deposited per time and aerosol concentration. This combined term is treated as a single modeled sink parameter that is constant with height up to the top of the canopy (except at the bottom cell where it includes the ground surface) and adjusted to match experimental data (Veranth et al., 2007). Since no vegetative deposition occurs above the canopy, $V_d A_V = 0$ above the canopy.

The gravitational settling velocity V_s is specified for Stoke's flow using the simple model outlined in Seinfeld and Pandis (1998) namely,

$$V_s = -\frac{1}{18}\frac{D_p^2 \rho_p g}{\mu}. \qquad (2)$$

Here, g is the gravitational acceleration constant (9.81 m-s^{-2}), ρ_p ,the density of the particle (taken as 2500 kg m^{-3} Nickovic et al., 2001) and μ, the dynamic viscosity of air (specified as 1.8×10^{-5} kg m s^{-1}). The model is valid for particle diameters in the range of $1\mu m \le D_p \le 20\mu m$. For the simulations described in this work, a particle diameter of $7\mu m$ was used as the mass mean diameter of typical soil dust PM_{10}.

2.3. Mean wind flow model

For this work, a model that utilizes simple boundary layer parameterizations to include the effects of rough-wall canopy drag is implemented. The canopy drag model is essentially a simplification of the (Macdonald, 2000) urban canopy model that was based on the work of (Cionco, 1965). For the canopy model, the user is only required to input the height of the vegetation H_{can}, an upstream mean reference velocity u_{ref} at the reference height z_{ref}, the upstream aerodynamic roughness length, z_o, the Monin-Obukhov length scale, L and a roughness specific attenuation coefficient a (described below). The upstream boundary layer profile is assumed to be logarithmic and calculated as:

$$\frac{u(z)}{u_{ref}} = \frac{\ln\left(\frac{z}{z_o}\right) - \psi\left(\frac{z}{L}\right)}{\ln\left(\frac{z_{ref}}{z_o}\right) - \psi\left(\frac{z}{L}\right)}. \qquad (3)$$

The measure of atmospheric stability used here is the Monin-Obukhov length scale $L = u_*^3 / \left[\kappa Q_o \left(g / T_o\right)\right]$, where T_o and Q_o are the surface temperature (K) and kinematic heat flux respectively (mKs^{-1}), u_* is the friction velocity (m-s^{-1}) and $\kappa = 0.41$ is the von Karman constant. The stability parameters in Eq. 3 are given by (e.g., Arya 2001):

$$\psi(z/L) = -5\left(\frac{z}{L}\right) \qquad z/L \geq 0 \qquad \text{Neutral and Stable}$$

$$\psi(z/L) = \ln\left[\left(\frac{1+x^2}{2}\right)\left(\frac{1+x}{2}\right)^2\right] - 2\tan^{-1} x + \frac{\pi}{2} \qquad z/L < 0 \qquad \text{Unstable}$$

where, $x = \left(1 - 15(z/L)\right)^{1/4}$. Using the input specified for the upstream boundary layer parameters, an estimate for the upstream friction velocity is made by rewriting the previous equation in the form

$$u(z) = \frac{u_*}{\kappa}\left[\ln\left(\frac{z}{z_o}\right) - \psi\left(\frac{z}{L}\right)\right], \qquad (4)$$

and solving for u_*. As a first approximation, it is assumed that the upstream u_* and z_o values apply in the displaced log layer above the canopy. The velocity in the displaced log layer is given by the following equation:

$$u(z) = \frac{u_*}{\kappa}\left[\ln\left(\frac{z-d}{z_o}\right) - \psi\left(\frac{z-d}{L}\right)\right]. \qquad (5)$$

To complete the solution, the velocity at the canopy height within the vegetation $u_{Hcan} = u\left(z = H_{can}\right)$ and the displacement height, d must be calculated. For simplicity, we assume that the flow within the canopy is independent of atmospheric stability and follow (Cionco, 1965), assuming that an exponential solution applies within the canopy and that the displaced log profile applies above the canopy. The exponential solution is given by

$$u(z) = u_{Hcan} \exp\left[a\left(\frac{z}{H_{can}} - 1 \right) \right]. \tag{6}$$

Here, *a* is the attenuation coefficient associated with specific types of roughness (Cionco, 1978). Larger values of *a* indicate an increased momentum sink associated with the roughness. The attenuation coefficient is dependant on a wide range of factors including: the flexibility, the shape, surface area and spacing of the roughness elements(Cionco, 1965). Typical values of *a* for different types of vegetation are provided in Table 1. Some generalizations for the calculation of the attenuation coefficient exist such as (Macdonald, 2000) for idealized building arrays and (Cionco, 1965) for vegetation. Generally, however, *a* values must be obtained by measuring velocity profiles within the canopy and fitting an exponential solution to them.

Up to this point, the method is very similar to the technique proposed by (Macdonald, 2000). Here we diverge from Macdonald's method by forcing the velocities and the slopes of the velocity profiles to be matched at the canopy height H_{can}. This simplifies Macdonald's method by eliminated a matching layer and fixes the values of d and u_{Hcan}. The displacement height d and u_{Hcan} are then obtained by solving the following two equations:

$$\frac{H_{can}}{H_{can} - d} \phi\left(\frac{H_{can} - d}{L} \right) = a \frac{u_H \kappa}{u_*} \tag{7}$$

$$u_{Hcan} = \frac{u_*}{\kappa} \ln\left(\frac{H_{can} - d}{z_o} \right) - \psi\left(\frac{H_{can} - d}{L} \right). \tag{8}$$

Where the universal stability functions are given by (Arya 2001) as:

$$\phi\left(\frac{z-d}{L}\right)=1+5\left(\frac{z-d}{L}\right) \qquad z/L \geq 0 \qquad \text{Neutral and Stable}$$

$$\phi\left(\frac{z-d}{L}\right)=\left(1-15\frac{z-d}{L}\right)^{-1/4} \qquad z/L < 0 \qquad \text{Unstable}$$

Since Eq. 7 and are not explicit in d , a numerical method is required in to obtain a solution. For the solutions given here, a simple iterative bisection method was used (Chapra and Canale, 2006). Figure 2 shows an example of three different velocity profiles with identical input parameters except for upstream stability.

2.4. Turbulence model

The vertical turbulent flux of particle concentration within the vegetation is modeled using a simple gradient method, namely

$$-\overline{w'c'}=K_{zz}\frac{\partial c}{\partial z}$$

as shown in Eq. 1. In the present model, it is assumed that the concentration diffusion coefficient K_{zz} is the same as the momentum diffusion coefficient. Hence, upstream of the canopy a simple log law boundary layer model is used where K_{zz} is specified based on Monin-Obukhov similarity as

$$K_{zz}=\frac{\kappa u_* z}{\phi(z/L)}. \tag{9}$$

Within the canopy, a mixing length model that is independent of atmospheric stability is assumed and specified in the form:

$$-\overline{u'w'} = l^2\left(\frac{\partial u}{\partial z}\right)^2 = K_{zz}\frac{\partial u}{\partial z}. \qquad (10)$$

In Eq. 10, the velocity gradient is calculated directly using finite differences from the mean flow field. Above the canopy, the mixing length scale is modeled as the sum of the canopy length scale (l_{cu}) and the surface layer length scale (l_{sl}) (i.e. $l = l_{cu} + l_{sl}$), where the mixing length l_{sl} is given by

$$l_{sl} = \frac{k(z-d)}{\phi\left(\frac{z-d}{L}\right)}. \qquad (11)$$

Within the canopy, the mixing length is broken up into an upper l_{cu} ($z/H_{can} > 0.3$) and lower l_{cl} ($z/H_{can} \le 0.3$) canopy mixing length following Cionco (1965). For $0.3H_{can} < z \le H_{can}$, the mixing length is assumed constant and modeled following (Macdonald, 2000) by substituting Eq. 6 into Eq. 10 and solving for the mixing length at $z = H_{can}$. This model assumes that the shear stress at the canopy height is the same as the shear stress in the surface layer. This yields the following approximation for the mixing length in the upper part of the canopy:

$$l_{cu} = \frac{H_{can}u_*}{au_{Hcan}}. \qquad (12)$$

For $z/H_{can} \le 0.3$, the mixing length is assumed to increase linearly from zero at the ground to the value predicted by Eq. 12 at $z/H_{can} = 0.3$. It should be noted that although the conditions in the canopy are assumed independent of stability, a dependence of stability is introduced by using the value of d obtained by matching the exponential and logarithmic curves as described in Section 2.3 above.

2.5 Numerical Implementation

The velocity parameterizations described above assume horizontal homogeneity. In the actual simulations, there was a finite fetch F between the road and the start of the roughness elements (see Fig. 1b). A rough wall turbulent boundary layer (Eq. 3, with z_o/H_{can} = 0.02) was assumed upwind of the vegetative canopy; the flow was immediately assumed to follow the canopy profiles parameterizations within the vegetation. To deal with this discontinuity, the initial flow field was forced to be mass consistent via a classical variational analysis procedure (Sherman, 1978). The resulting mass consistent wind field and turbulence models described above were input into a numerical simulation of Eq. 1 using Matlab subject to the following boundary conditions: $dc/dx = 0$ at the inlet and outlet; $dc/dz = 0$ at the top of the domain and $c = 0$ at the ground. The dust cloud was initialized with a uniform concentration of c_o = 75 mg-m^{-3} over a rectangular region centered on the road with a height H_{dc} and width W_{dc}. The height was varied throughout the simulations but the cloud width was fixed at 3 m corresponding to the width of a typical travel lane. The spatial domain was rectangular with a streamwise length of 630m and a height of 50m. The fetch F from the center of the road to the upwind edge of the domain was 30m for the simulations.

The spatial domain was discretized using finite volumes (Versteeg and Malalasekera, 1995). The advective terms were modeled by a first order upwind finite difference. The diffusive terms were modeled using second order central differences. The body terms are exact and the temporal dependence of Eq. 1 is modeled using an Alternating Direction Implicit (ADI) technique (Anderson, 1995). Variable time steps are used during a typical 125s simulation. Smaller time steps of the order of 0.01s are used in the first 10s. Larger time steps of the order of 0.25 to 1s are used for the rest of the simulation. To minimize computational effort, a non-uniform mesh is utilized by solving Eq. 1 on a logarithmic mesh (Anderson, 1995). The grid is stretched both in the vertical and horizontal directions with stretching factors of 0.07 and 0.004 respectively. The minimum grid sizes in vertical and horizontal directions were 5.6 cm and 50.8 cm. A typical simulation runs on a Celeron PC laptop in about two and half minutes. This involves about 30,000 nodes (300 in the streamwise direction and 100 in the vertical) and 500 time steps. The large number of time steps is necessary to ensure mass conservation of the dust particles. This is done by running each time step twice, once without vegetative deposition and another with vegetative deposition (Boybeyi, 2000; Schieffe and Morris, 1993).

3. Results

3.1. Turbulence Model

Figure 3 illustrates the performance of the mixing length model (Eq. 12) against a number of experimental data sets. The data set was compiled from a wide range of wind tunnel and field experiments described in the figure caption. An average value for the in-canopy mixing length was calculated directly from the available data sets using Eq. 10 and then compared to Eq. 12. With the exception of the (Seginer et al., 1976) wind tunnel study of flow through surface mounted cylinders, the data appear to be quite linear over the range $0.076 < u_* / \left(a u_{Hcan} \right) < 0.36$.

Linear regressions of the data yields a best fit of $l_{cu} / H_{can} = 0.7(u_* / au_{Hcan}) + 0.07$ with R^2 = 0.89. Hence, the model tends to under predict the mixing length in the canopy.

Figure 4 shows the modeled momentum fluxes in the canopy compared to measured fluxes separated into (a) low, (b) medium and (c) high attenuation coefficients. The model matches the data quite well in the upper 25% of the canopy, however in the lower 75%, the model can under predicts fluxes by as much as ~50%.

3.2. Road Dust Simulation

A number of factors determine the fraction of the initial dust cloud deposited onto roughness elements. In this work, we focus on the effects of roughness length, atmospheric stability and deposition effectiveness of the canopy. In order to maintain this focus, a test canopy with dimensions similar to a real unpaved road was implemented as described in section 2.5. In addition, the dimensionless initial dust cloud height was $H^* = H_{dc} / H_{can} = 2$ and a dimensionless fetch $F^* = F / H_{can} = 2$ was utilized. This example case is representative of relatively small bushes adjacent to an unpaved road (typical of an arid environment), but would not be representative of a dirt road near the edge of a tall forest where H^* and $F^* << 1$. Figure 5a shows the effect of three different attenuation coefficients on the mass fraction of suspended particles (M_s/M_o) as a function of dimensionless advection time for neutral atmospheric stability. Here M_o is the initial mass in the dust cloud and M_s in the mass remaining in the air at some later time. In this simulation, the deposition term $V_d A_V$ was held constant such that the effect of the modeled wind profile and turbulence within the canopy were isolated. As expected, more dense canopies result in higher attenuation coefficients, reduced wind speed within the canopy and enhanced deposition. Similarly, Fig. 5b shows the effect of atmospheric stability on a canopy with a moderate attenuation coefficient (a = 2.25). For the case shown (with 2 ms^{-1} wind speed upstream and 2 m tall canopy) 30 m downstream of the road, there is a 67% reduction in M_s/M_o for the stable atmospheric stability case compared to the unstable case.

4. Discussion

Understanding the effectiveness of particle deposition onto various types of roughness is of great importance. A bulk measure of this effectiveness that utilizes the methodology outlined in this paper can be obtained by considering the ratio of the turbulent diffusion time scale to a deposition time scale. Here, the deposition time scale refers to the horizontal deposition associated primarily with impaction of the dust cloud onto roughness elements (i.e. "filtering") and may be defined as $\tau_d = (V_d A_V)^{-1}$. The inverse of this deposition time scale is also referred to by (Veranth et al., 2007) as the clearance frequency because it represents the fraction of particles in a control volume that are removed per unit time by deposition to vegetation and other surfaces. Another time scale is associated with the time required for a particle to move out of the canopy (over a height H_{can}) through turbulent diffusion can be defined as $\tau_t = H_{can}^2 / K_{zz}(H_{can})$. The ratio of these two time scales is

$$\mathrm{T}^* = \frac{V_d A_V H_{can}^2}{K_{zz}(H_{can})} = \frac{\tau_t}{\tau_d} . \tag{13}$$

In Eq. 13, $K_{zz}(H_{can})$ is the turbulent diffusivity at the top of the canopy. T^* provides a bulk metric to determine the expected deposition rate effectiveness of a canopy associated with the horizontal advection of dust. T^* is dependent on the specific geometry of the canopy, particle deposition physics, as well as atmospheric turbulence. Considering the limits of T^* is particularly useful. As $\tau_t / \tau_d \to \infty$, we expect that the suspended mass fraction $M_s / M_o \to 0$ because most of the particles should be removed from the air stream before they diffuse out of the canopy.

Similarly, as $\tau_t / \tau_d \to 0$, M_s/M_o should approach the well mixed case where horizontal deposition is of little importance (e.g. far downwind in Fig. 1a) since the particulate cloud disperses rapidly compared to the time required to deposit particulate matter onto roughness elements. Figure 6 shows M_s/M_o as a function of the deposition rate effectiveness on a semi-log plot. The plot is composed of three distinct regimes: (1) $\mathrm{T}^* < 1$, turbulence rapidly mixes particles and the M_s/M_o decreases slowly with increasing T^*, (2) $1 < \mathrm{T}^* < 10$, the M_s/M_o decreases rapidly as the importance of deposition increases and (3) $\mathrm{T}^* > 10$, M_s/M_o begins to decrease more slowly in response to very low particle concentrations in the canopy.

Figure 7 shows the effect of the ratio of the initial dust cloud height to the vegetative canopy height, H^* on mass fraction suspended at equivalent non-dimensional times after the start of the simulations. As expected, for short dust clouds $H^* < 1$, much of the dust is removed as it is advected horizontally through the roughness elements. The mass fraction suspended rapidly increases with increasing H^* until $H^* \sim 4$ as the importance of the horizontal impaction on the roughness elements decreases. For $H^* > 4$, horizontal removal is insignificant and the problem approaches the classical well mixed vertical deposition onto a surface case.

Figure 8 summarizes the model's utility to help describe the effect of roughness and atmospheric stability on deposition in vegetative or building canopies. For highly unstable atmospheric conditions, significant changes in roughness result in very small changes in deposition. While for stable atmospheric conditions, relatively small increases in roughness result in significantly enhanced deposition. For example, consider the hypothetical canopy with an attenuation coefficient of 2.5 shown in Fig. 8. The decrease in M_s/M_o from z/L = -2 to z/L = -0.5 is less than

~8%, while the decrease from z/L = 0.5 to z/L = 2 is ~35%. In addition, Figure 8 helps explain the discrepancy between the convective low vegetation Ft. Bliss results and the high roughness stable conditions for the Dugway Proving Ground experiment described in the introduction. The Ft. Bliss case would reside in the lower left corner of Fig. 8 where deposition is least, while the Dugway case would be in the upper more central part of the figure where deposition is substantially increased.

One of the advantages of using the Eulerian transport model given in Eq. 1, is that it allows one to analyze and understand the contribution of each of the terms to the total transport. Figure 9 shows the contributions of the various terms from Eq. 1 twenty meters downwind of the leading edge of the canopy with most of the plume still contained within the vegetation. Figure 9a shows the contribution of the plume 20 seconds after the start of the simulation. As expected, the deposition term (term *V*) is always a sink within the canopy (ie. negative values) and zero above. The other three terms on the right hand side of Eq. 1(term *II*, *III* and *IV*) may be positive or negative depending on vertical location and time. As shown in Fig. 9a, the mean streamwise advection is the dominant transport term. The sign of the advection term is positive near the ground ($0<z/H_{can}<0.14$) and negative for $z/H_{can} > 0.14$. Since the velocities are nearly constant in the streamwise direction, the advection term is dominated by the streamwise gradient of the concentration. Hence, where term *II* is positive, the concentration is increasing with streamwise distance and where term *II* is negative, the concentration must be decreasing. Due to the directional behavior of advection, this is equivalent to stating that at higher elevations the dust plume is advected downwind at a greater rate than at the bottom of the the canopy where velocities are very low. That is, the higher locations are observing the departure of the bulk of the dust plume, while lower heights are still observing the cloud’s arrival.

The vertical turbulent diffusion (term *III*) is dependent on the gradient of the product of the local vertical concentration gradient and *Kzz*. Since *Kzz* increases monotonically, term *III* follows the curvature of the concentration profile. Hence, term *III* is positive below the lowest inflection point in the concentration profile (z/H_{can}<0.1), negative from 0.1<z/H_{can}<0.22 and positive again z/H_{can}>0.22. This is intuitively expected, as the concentration will decreases near the peak and increase at the tails due to diffusion. Since the settling velocity V_s is constant for a given simulation (one particle size and type), the gravity settling (term *IV*) is only a function of the concentration gradient. Hence, for small particles, term *IV* takes on small positive values below the peak and negative values above the peak.

4. Conclusions

In this paper, we describe the development of a quasi-2D Eulerian atmospheric diffusion model applied to the transport and deposition of fugitive dust near an unpaved road. Specifically, this work addresses a gap in the literature associated with transport and deposition in the "impact zone" where horizontal deposition may be of importance. The primary attribute of the present modeling technique is that a user can investigate the effects of various deposition scenarios associated with different roughness and atmospheric stabilities, while only needing to supply a small the number of difficult to obtain input parameters. Since the model also runs rapidly, a large number of cases can be run parametrically to investigate the importance various input variables; allowing decision makers more information regarding planning scenarios.

The model also provides insight toward reconciling the differences between field experiments in the literature where large differences were observed in deposition rates for different stabilities and canopy roughnesses. The primary limitation of the model is the ability to accurately determine the vegetative deposition parameter or so-called clearance frequency. To understand the clearance frequency better, a dimensionless parameter called the transport effectiveness is identified and the limiting cases discussed. In general, the model captures the essential physics of near source dust transport and provides a tool that that can efficiently simulate site-specific conditions in practical situations.

Acknowledgements

This work was sponsored by the Strategic Environmental Research and Development Program project CP1190 and by Southwest Center for Environmental Research and Policy project A-02-7 and A-04-03. We also wish to thank Mr. Thomas Booth for his hard work and contributions to the mean wind model.

References:

Anderson, J.D., 1995. Computational fluid dynamics. McGraw Hill, New York, 547 pp.

Aylor, D.E. and Flesch, T.K., 2001. Estimating spore release rates using a Lagrangian stochastic simulation model. J. Appl. Meteor., 40(7): 1196-1208.

Belcher, S.E., 2005. Mixing and transport in urban areas. Phil. Trans. R. Soc. A, 363: 2947-2968.

Boybeyi, Z., 2000. Mesoscale atmospheric dispersion. WIT Press, Boston, 448 pp.

Britter, R.E. and Hanna, S.R., 2003. Flow and dispersion in urban areas. Annu. Rev. Fluid Mech., 35: 469-496.

Brunet, Y., Finnigan, J.J. and Raupach, M.R., 1994. A wind tunnel study of air flow in waving wheat: single-point velocity statistics. Bound.-Layer Meteor., 70: 95-132.

Chamberlain, A.C., 1975. The movement of particles in plant communities. Vegetation and the Atmosphere, 1: 155-203.

Chapra, S.C. and Canale, R.P., 2006. Numerical Methods for Engineers. McGraw Hill, New York.

Cionco, R.M., 1965. Mathematical model for air flow in vegetative canopy. J. Appl. Meteorol., 4: 517-522.

Cionco, R.M., 1978. Analysis of canopy index values for various canopy densities. Boundary-Layer Meteorology, 15(1): 81-93.

Davidson, C.I., Phalen, R.F. and Solomon, P.A., 2005. Airborne Particulate Matter and Human Health: A Review. Aerosol Science & Technology, 39(8): 737-749.

Denmead, O.T. and Bradley, E.F., 1987. On scalar transport in plant canopies. Irrig. Sci., 8: 131-149.

Etyemezian, V. et al., 2004. Deposition and removal of fugitive dust in the arid southwestern United States: measurements and model results. J. Air Waste Manag. Assoc., 54(9): 1099-1111.

Finnigan, J.J., 2000. Turbulence in plant canopies. Annu. Rev. Fluid Mech., 32: 519-571.

Harley, R.A., Hunts, S.E. and Cass, G.R., 1989. Strategies for the control of particulate air quality: least-cost solutions based on receptor-oriented models. Environmental Science & Technology, 23(8): 1007-1014.

Harman, I.N. and Finnigan, J.J., 2007. A simple unified theory for flow in the canopy and roughness sublayer. Boundary-Layer Meteorology, 123(2): 339-363.

Kaimal, J.C. and Finnigan, J.J., 1994. Atmospheric Boundary Layer Flows: Their Structure and Measurement. Oxford University Press US.

Kastner-Klein, P. and Rotach, M.W., 2004. Mean flow and turbulence characteristics in an urban roughness sublayer. Bound.-Layer Meteor., 111: 55-84.

Macdonald, R.W., 2000. Modelling the mean velocity profile in the urban canopy layer. Bound.-Layer Meteor., 97: 25-45.

Nicholson, K.W., 1988. The dry deposition of small particles: A review of experimental measurements. Atmospheric Environment, 22(12): 2653-2666.

Nickovic, S., Kallos, G., Papadopoulos, A. and Kakaliagou, O., 2001. A model for prediction of desert dust cycle in the atmosphere. Journal of Geophysical Research, 106(D16): 18113-18130.

Novak, M.D., Warland, J.S., Orchansky, A.L., Ketler, R. and Green, S., 2000. Wind Tunnel And Field Measurements Of Turbulent Flow In Forests. Part I: Uniformly Thinned Stands. Bound.-Layer Meteor., 95(3): 457-495.
Pace, T.G., 2005. Methodology to estimate the transportable fraction (TF) of fugitive dust emissions for regional and urban scale air quality analyses, USEPA.
Poggi, D., Porporato, A., Ridolfi, L., Albertson, J.D. and Katul, G.G., 2004. The effect of vegetation density on canopy sub-layer turbulence. Bound.-Layer Meteor., 111: 565-587.
Ramaswami, A., Milford, J.B. and Small, M.J., 2005. Integrated environmental modeling: pollutant transport, fate and risk in the environment. Wiley, 678 pp.
Raupach, M.R., P.A., C. and Legg, B.J., 1986. Experiments on scalar dispersion within a model plant canopy. Part I: The turbulence structure. Bound.-Layer Meteor., 35(21-52).
Raupach, M.R. and Thom, A.S., 1981. Turbulence in and above plant canopies. Annu. Rev. Fluid Mech., 13: 97-129.
Raupach, M.R., Woods, N., Dorr, G., Leys, J.F. and Cleugh, H.A., 2001. The entrapment of particles by windbreaks. Atmos. Environ., 35: 3373-3383.
Schieffe, R.D. and Morris, R.E., 1993. A review of the development and application of the urban airshed model. Atmos. Environ., 27B: 23-29.
Seginer, I., Mulhearn, P.J., Bradley, E.F. and Finnigan, J.J., 1976. Turbulent flow in a model plant canopy. Bound.-Layer Meteor., 10: 423-453.
Sehmel, G.A., 1980. Particle and gas dry deposition- A review. Atmospheric Environment, 14(9): 983-1011.
Seinfeld, J.H. and Pandis, S.N., 1998. Atmospheric chemistry and physics - from air pollution to climate change. Wiley, Hoboken, 1203 pp.
Shaw, R.H., Silversides, R.H. and Thurtell, G.W., 1974. Some observations of turbulence and turbulent transport within and above plant canopies. Bound.-Layer Meteor., 5: 429-449.
Sherman, C.A., 1978. A mass-consistent model for wind fields over complex terrain. J. Appl. Meteor., 17(3): 312-319.
Slinn, W.G.N., 1982. Predictions for particle depostion to vegetative canopies. Atmos. Environ., 16: 1785-1794.
Veranth, J.M., Pardyjak, E.R. and Seshadri, G., 2003. Vehicle-generated Dust Transport: Analytic Models and Field Study. Atmos. Environ., 37: 2295-2302.
Veranth, J.M., Speckart, S.O., Yin, F., Etyemezian, V. and Pardyjak, E.R., 2007. Near-source deposition of vehicle-generated fugitive dust on vegetative surfaces and buildings, part II: Field deposition measurements and model validation submitted to Atmos. Environ.
Versteeg, H.K. and Malalasekera, W., 1995. An introduction to computational fluid dynamics– the finite volume approach. Longman Scientific & Technical, 257 pp.
Watson, J.G. and Chow, J.C., 1994. Clear sky visibility as a challenge for society. Annu. Rev. Energy Environ., 19: 241-266.
Watson, J.G. and Chow, J.C., 2000. Reconciling Urban Fugitive Dust Emissions Inventory and Ambient Source Contribution Estimates: Summary of Current Knowledge and Needed Research. DRI Document.
Wilson, J.D., Ward, D.P., Thurtell, G.W. and Kidd, G.E., 1982. Statistics of atmospheric turbulence within and above a corn canopy. Bound.-Layer Meteor., 24: 495-519.

Table 1. Table of the various experimental data used in Figures 3 and 4. WT indicates wind tunnel measurements and Field indicates measurements that were acquired at full scale in the field. Note that the Moga forest data (originally acquired by Brunet, but unpublished) were adapted directly from (Kaimal and Finnigan, 1994).

Canopy Type	Experiment	Reference	Attenuation Coefficient *a*	Symbol
Urban	WT	(Kastner-Klein and Rotach, 2004)	1.26	●
Triangular cylinders	WT	(Novak et al., 2000)	1.3	▲
Square cylinders	WT	(Novak et al., 2000)	2.0	◇
Square cylinders	WT	(Poggi et al., 2004)	1.0	■
Rectangular cylinders	WT	(Raupach et al., 1986)	0.84	×
Circular cylinders	WT	(Novak et al., 2000)	3.0	+
Circular cylinders	WT	(Seginer et al., 1976)	1.7	●
Wheat	WT	(Brunet et al., 1994)	1.6	◆
Corn field	Field	(Shaw et al., 1974)	2.4	▲
Corn field	Field	(Wilson et al., 1982)	4.1	△
Moga forest	Field	(Kaimal and Finnigan, 1994)	1.7	■
Bordeaux forest	Field	(Brunet et al., 1994)	3.2	□
Uriarra forest	Field	(Denmead and Bradley, 1987)	1.7	○

(a)

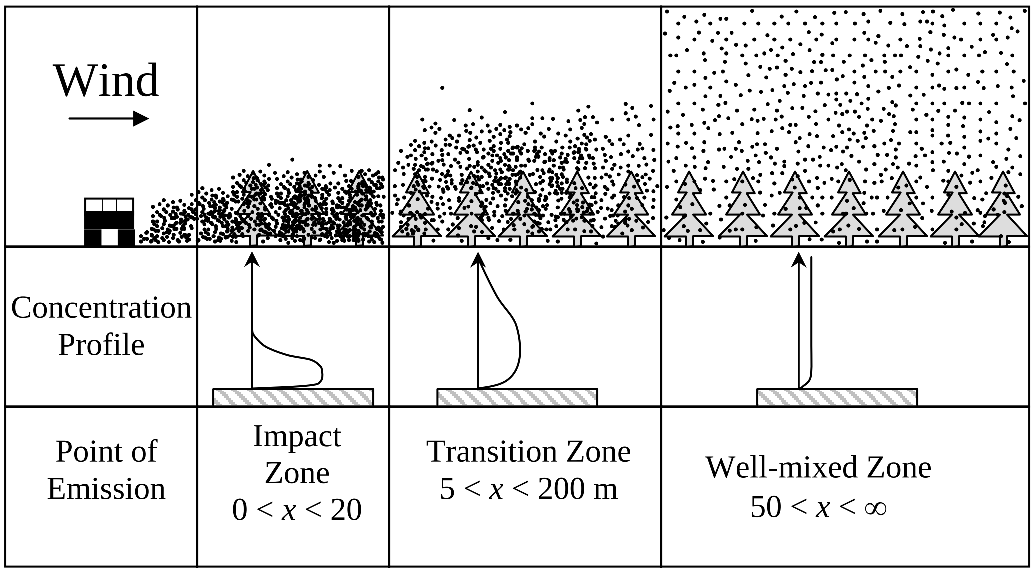

(b)

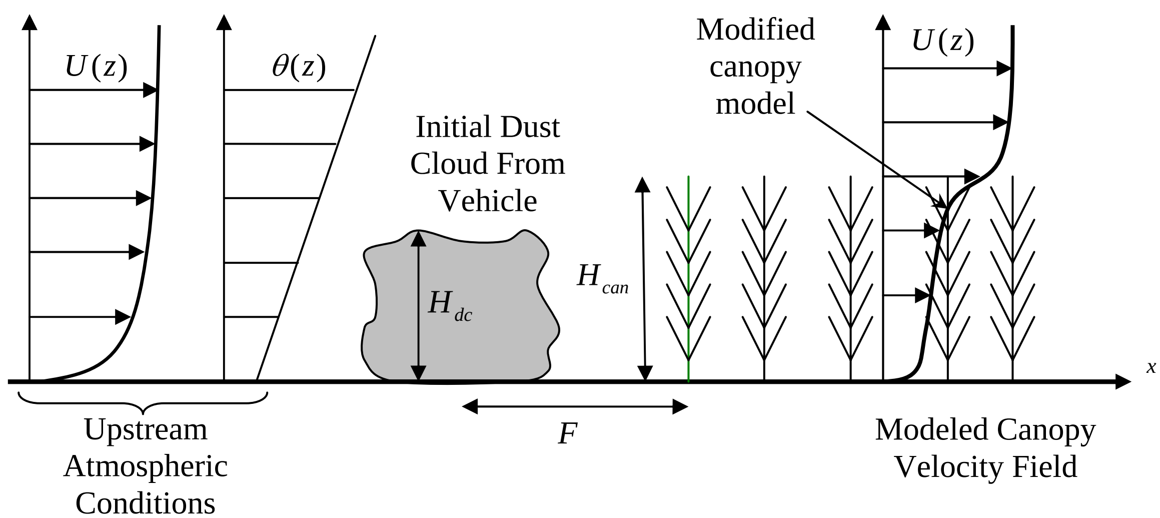

Figure 1. (a) Limiting cases in dust transport (adapted from Etyemezian et al. 2004). (b) Schematic defining the basic fugitive dust cloud problem in the impact zone.

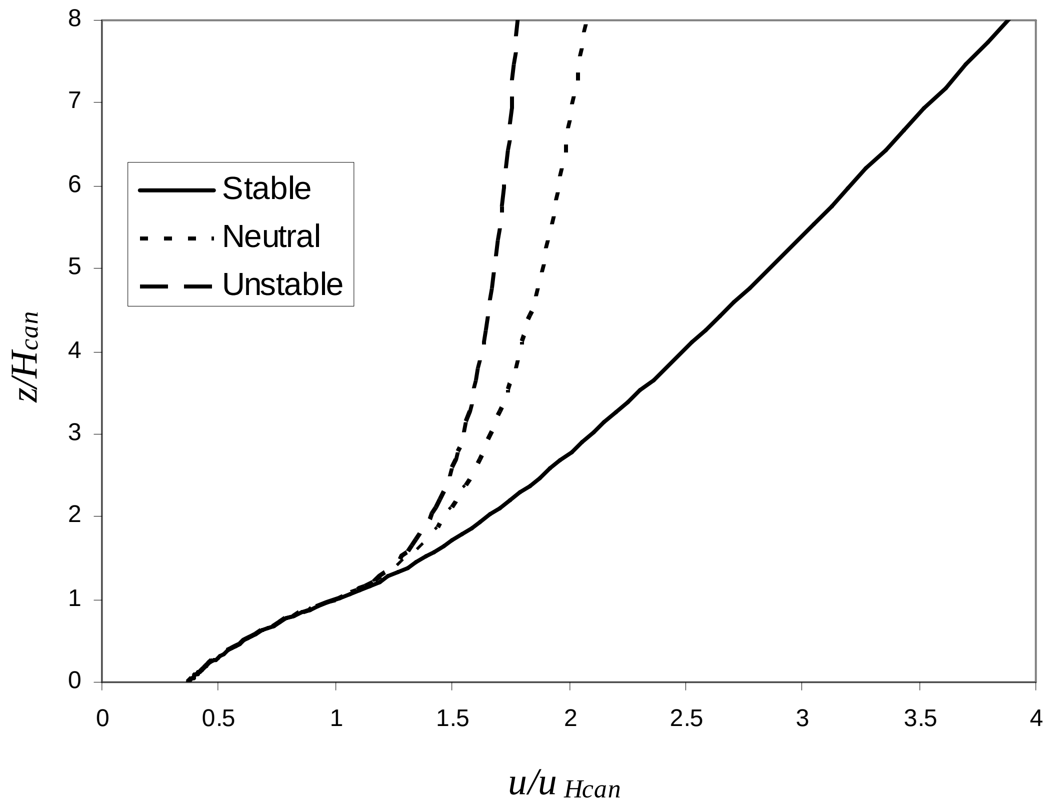

Figure 2. Mean wind speed profiles using the model described in the text. For these calculations the attenuation was taken as a = 1 and the dimensionless stability parameters for the stable and unstable cases where H_{can}/L = 0.2 and H_{can}/L = -0.2 respectively.

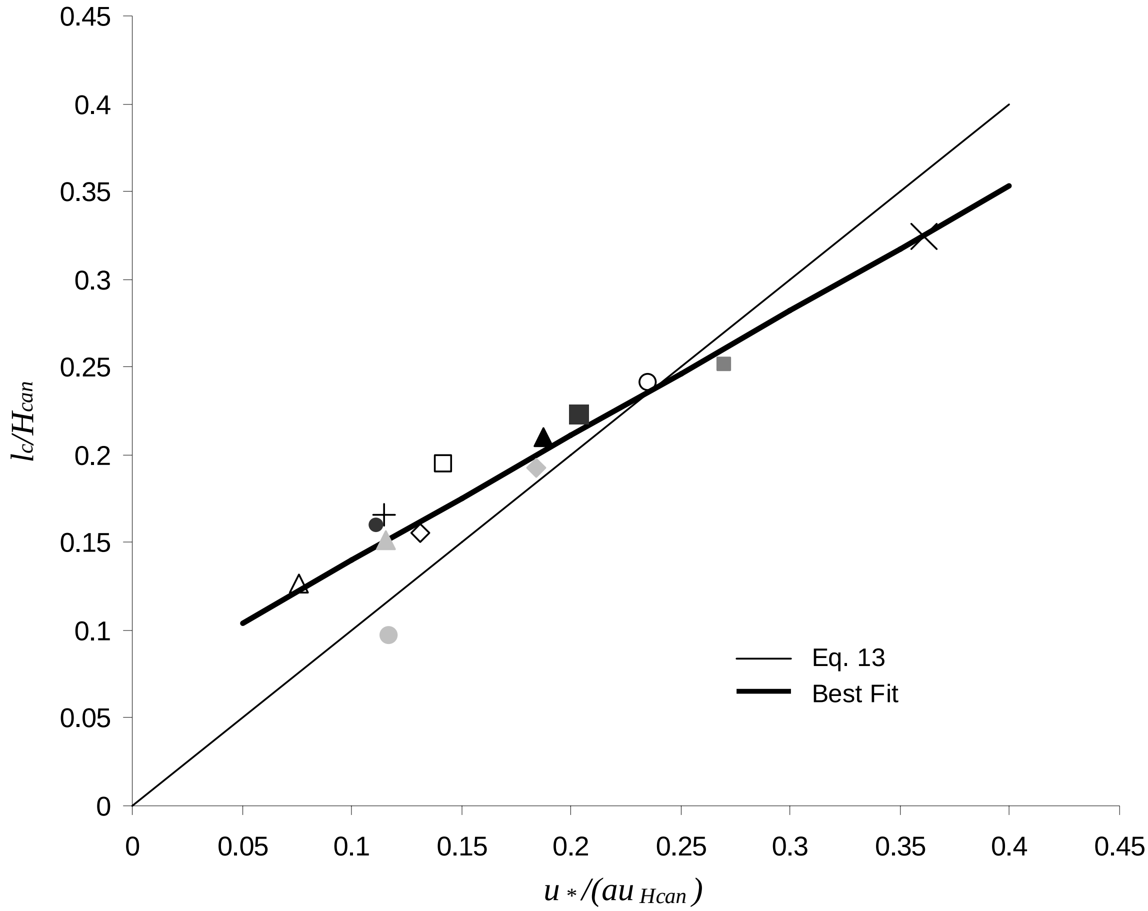

Figure 3. Dimensionless mixing length model (Eq. 12) plotted with data from various roughness sources. The equation of the best fit line is given by $l_{cu}/H_{can} = 0.7(u_*/au_{Hcan}) + 0.07$ with R^2 = 0.89. Definitions of the symbols are given in Table 1.

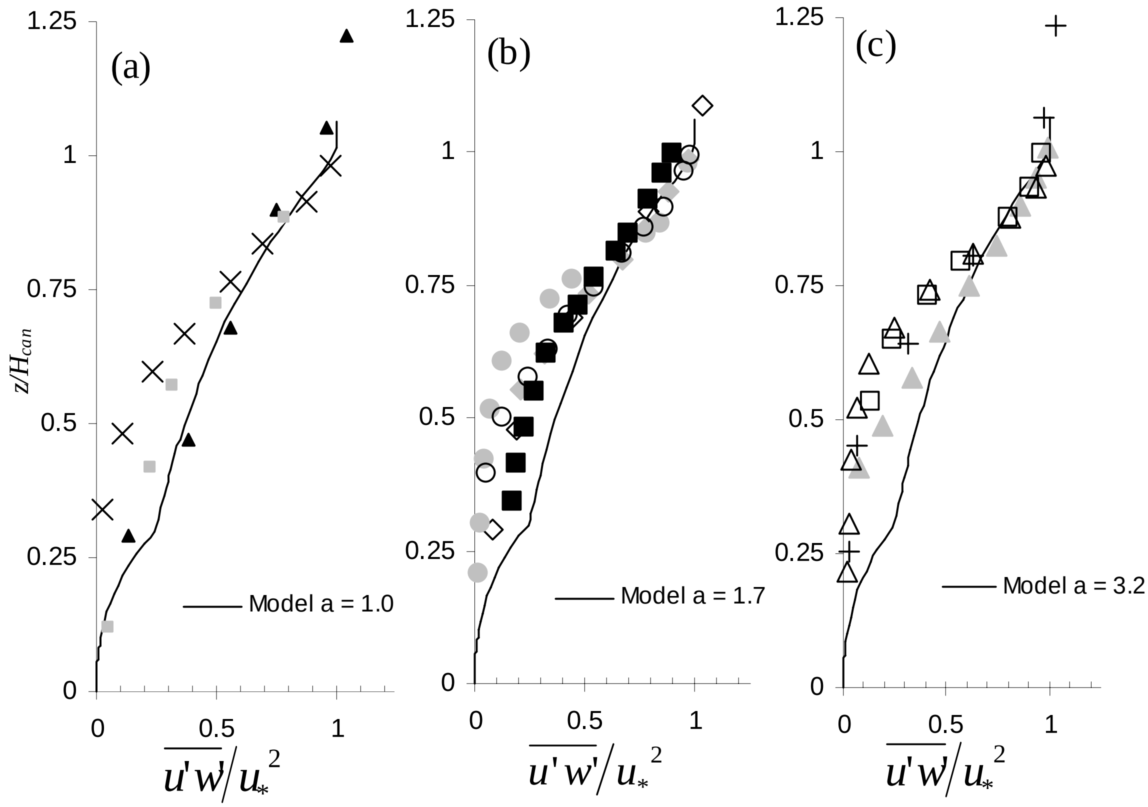

Figure 4. Modeled and experimental vertical profiles of the normalized momentum flux for (a) lower $0.84 \le a \le 1.3$, (b) moderate $1.6 \le a \le 2.0$ and (c) higher $2.4 \le a \le 4.1$ attenuation coefficients. Definitions of the symbols are given in Table 1.

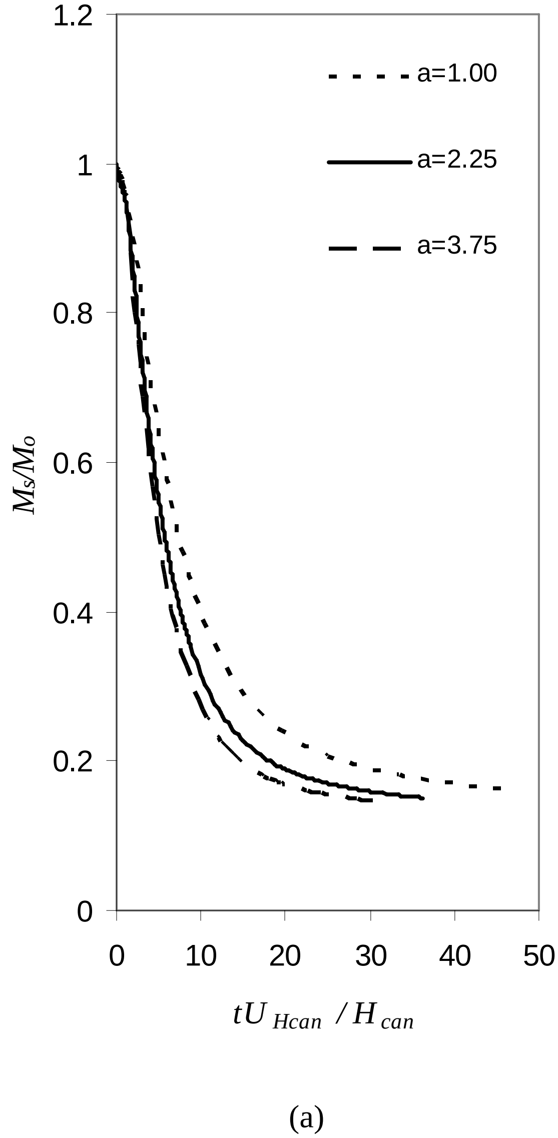

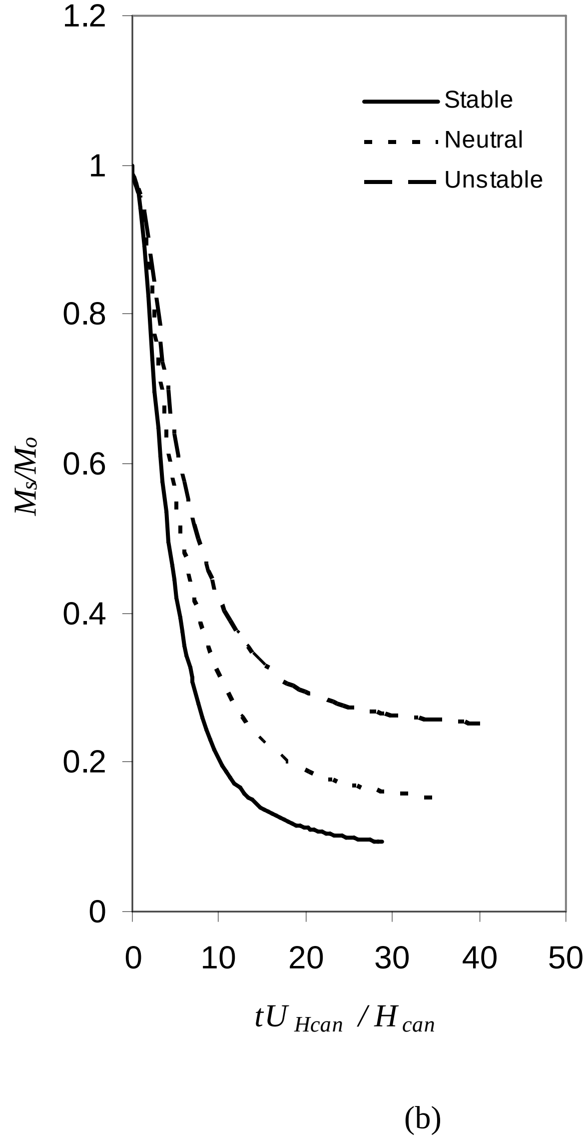

Figure 5. Mass fraction of suspended particles as a function of non-dimension advection time for (a) three canopies with different attenuation coefficients (and corresponding T^* = 8.5, 17, 27 for a = 1.0, 2.25 and 3.75) and neutral stability; (b) and for a canopy with a = 2.25 and T^* = 17 with different atmospheric stabilities (stable: H_{can}/L = 0.2, unstable: H_{can}/L = -0.2).

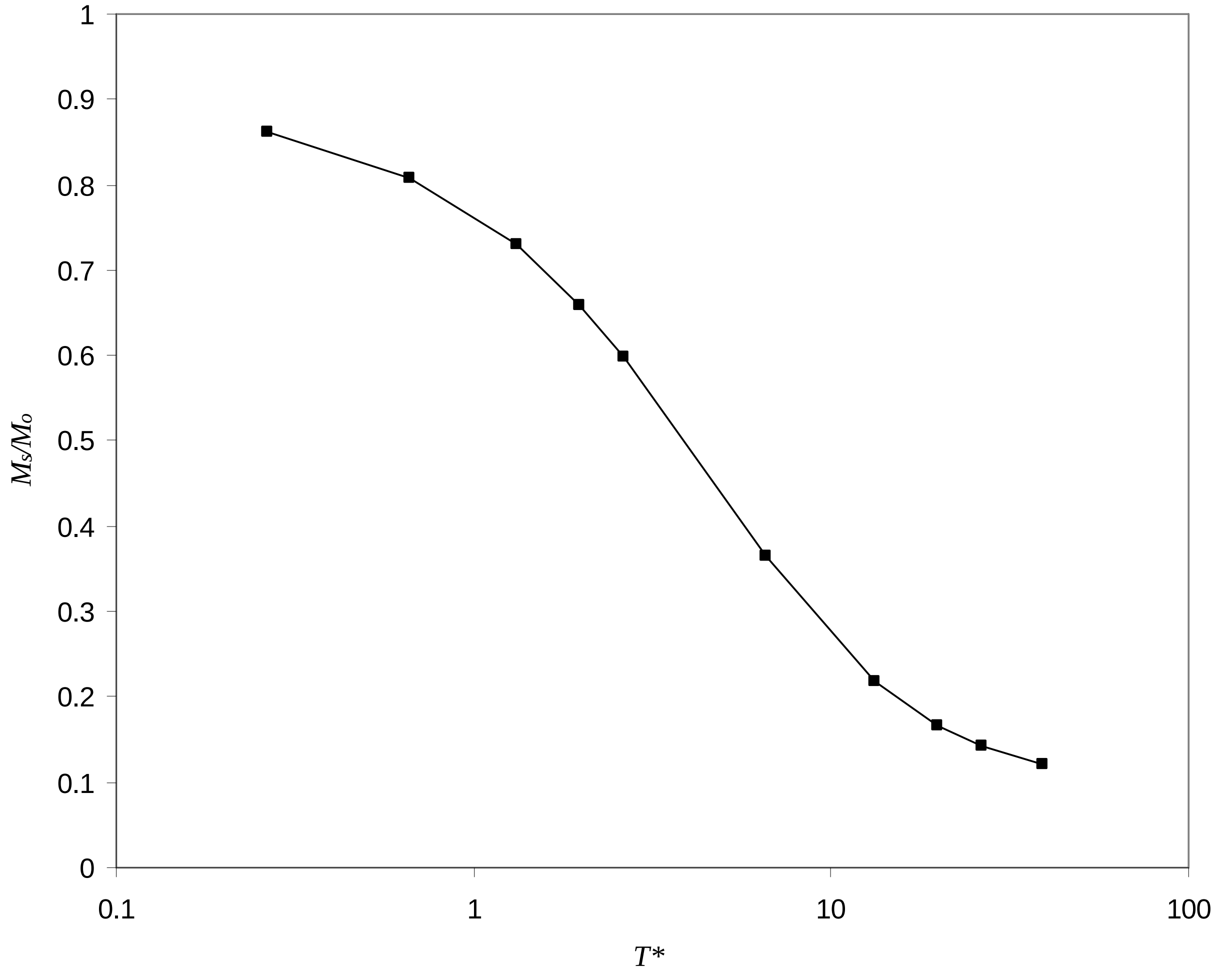

Figure 6. Mass fraction of suspended particles as a function of the deposition rate effectiveness for different atmospheric stabilities (a = 2.25, F^* = 2, H^* = 1, $u_{Hcan}t / H_{can} = 20$). Note that as T^* approaches zero M_s/M_o should approach the fraction suspended for flow over a flat wall.

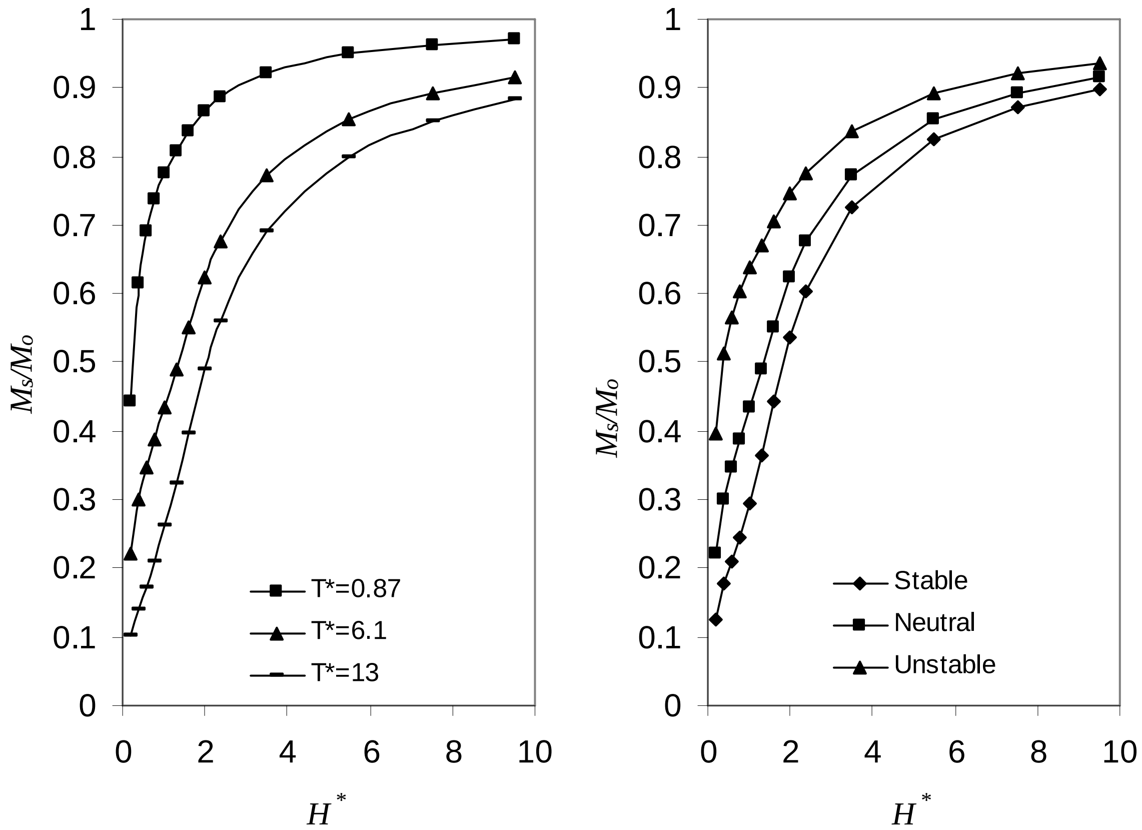

(a) (b)

Figure 7. Mass fraction of suspended particles as a function of dimensionless dust cloud height for (a) varying deposition effectiveness (neutral stability, a = 2.25, F^* = 2, tU_{Hcan}/H_{can} = 10) and (b) varying atmospheric stability (a = 2.25, F^* = 2, tU_{Hcan}/H_{can} = 10, T^* = 6.1).

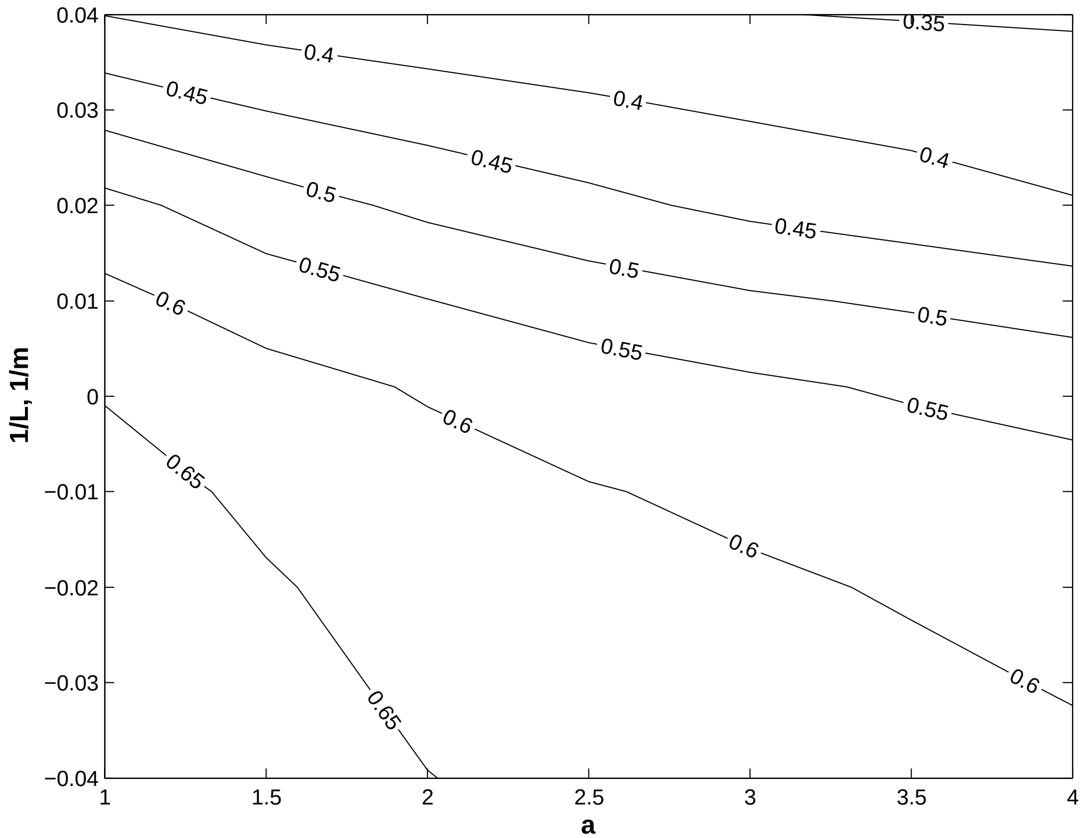

Figure 8. Contour plot Illustrating the effect of atmospheric stability and roughness on mass fraction of suspended particles for a hypothetical vegetative canopy ($H^* = 1$, $A_v V_d = 0.01\ s^{-1}$, $F^* = 2$, $tU_{Hcan}/H_{can} = 20$).

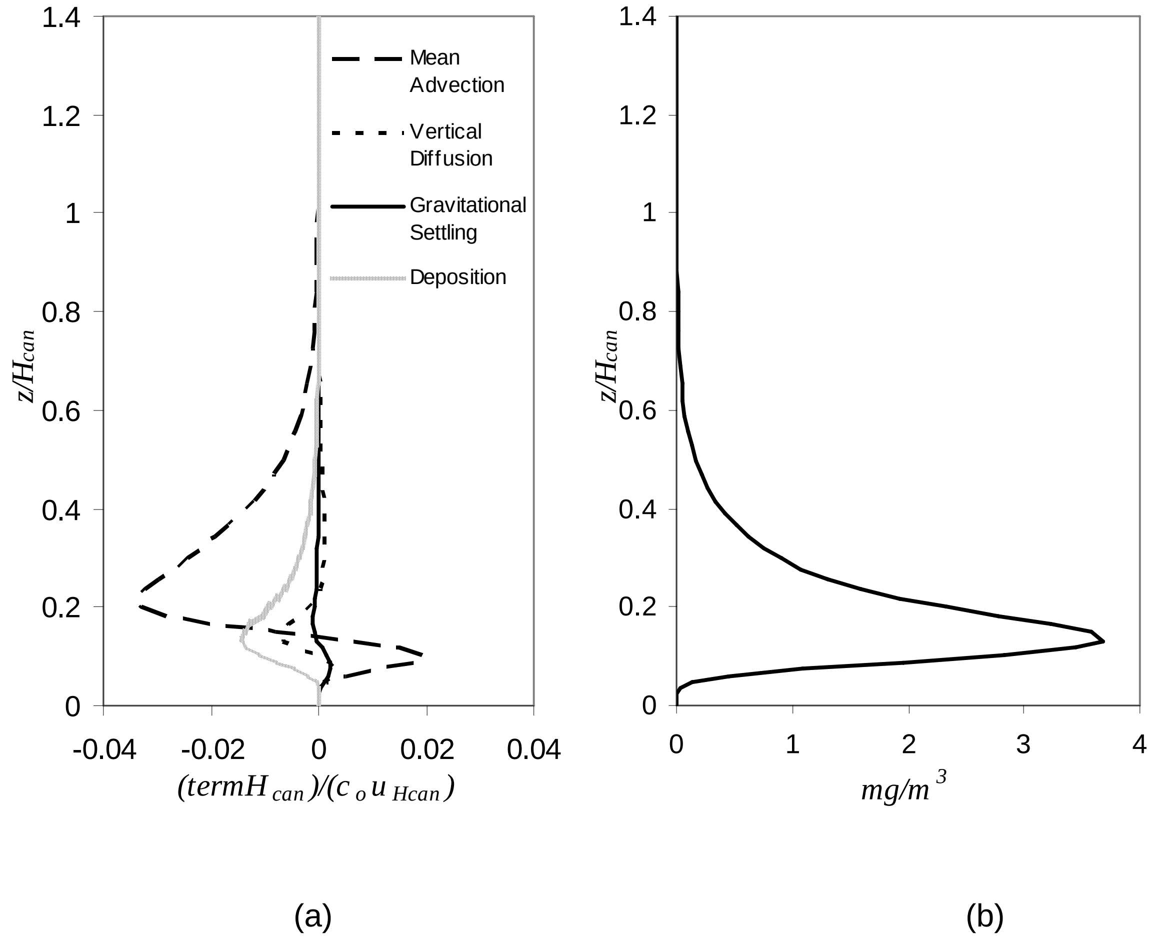

Figure 9. (a)Non-dimensional vertical variation of the various terms at an instant of time in the two-dimensional transport equation, Eq. 2 (a = 2.25, H^* = 1, F^* = 2, T^* = 22, tU_{Hcan}/H_{can} = 6).(b) Vertical Concentration profile normalized by the initial concentration at identical time, t = 20 s and location x = 20 m.

APPENDIX 2

Near-source Deposition of Vehicle-Generated Fugitive Dust on Vegetation and Buildings Part 2: Field Measurements and Model Validation

Authors and Affiliations

John M. Veranth[1], Scott O. Speckart[2], Fang Yin[3], Vic Etyemezian[4], Eric R. Pardyjak[2]

1. Department of Pharmacology and Toxicology, University of Utah, Salt Lake City, Utah

2. Department of Mechanical Engineering, University of Utah, Salt Lake City, Utah

3. Department of Chemical Engineering, University of Utah, Salt Lake City, Utah

4. Atmospheric Sciences Division, Desert Research Institute, Las Vegas, Nevada

Manuscript for Submission to
Atmospheric Environment
October 16, 2007

Corresponding Author Contact Information

John M. Veranth
Department of Pharmacology and Toxicology, University of Utah
30 South 2000 East, Room 112 Skaggs Hall
Salt Lake City, UT 84112-5820
Phone: 801-581-3789
Fax: 801-585-5111
Email: John.Veranth@utah.edu

Abstract

The near-source removal of vehicle-generated fugitive dust was studied by deposition measurements on test surfaces and by computational simulations to improve the scientific basis for effective air quality management strategies. Deposition was measured under summer and winter meteorological conditions using on both artificial vegetation and flat substrates. Deposition velocity calculated from aerosol concentration and scanning electron microscopy imaging of polycarbonate substrates that had been exposed while facing in orthogonal directions was approximately isotropic suggesting that impaction and interception due to advection and small-scale turbulence are important. A computational model for fugitive dust deposition, described in the companion Part 1 paper, was used to reanalyze data from two published field studies that compared dust flux adjacent to an unpaved road versus approximately 100 m downwind. The model considers deposition velocity, effective deposition surface area, the height of the canopy, and wind profile. Model simulation results were compared to field measurements and the effects of alternative site conditions are summarized. Canopy height relative to the initial dust cloud height, the area of surface roughness available for deposition, and the atmospheric stability are predicted to affect the partitioning of the initially suspended dust between transport and near-source redeposition. This work supports the hypothesis that the accuracy of emission inventory-based air quality modeling of fugitive dust can be improved by including an adjustment for near-source deposition.

Introduction

Vehicle-generated fugitive dust is a major source of ambient particulate matter (PM) in dry climates creating a health risk for sensitive individuals living near unpaved roads, and contributing to visibility impairment from haze. Developing scientifically valid models for predicting ambient fugitive dust is a major concern for air quality managers in the western United States because of the regional visibility protection rule requiring reasonable progress toward the goal of restoring natural visibility in the National Parks. (Code of Federal Regulations 2006) Recent efforts initiated by air quality agencies have improved the understanding of local- and regional-scale dust emission inventories and dust control strategies, (Watson 2002; Western Regional Air Partnership Dust Emissions Forum 2006) but the transport and removal of suspended dust in the near-source region is still poorly understood.

A systematic discrepancy has been observed between the predicted geological dust contribution based on emission inventories and the amount of inorganic minerals actually found in air samples at receptor sites (Watson and Chow 2000). A hypothesis to explain this discrepancy is that the inventories overstate the contribution of geological dust to ambient PM because not all suspended dust is transported a sufficient distance to affect air quality. Alternative explanations for the observed discrepancy include systematic bias in the emission factors used for model input, uncertainty in receptor-based source apportionment models, and differences in the dominant sources for most polluted days compared to annual averages.

Two recent field studies published measurements of the change in dust flux in the first 100 m downwind of an unpaved test road (Etyemezian, Ahonen et al. 2004; Etyemezian, Gillies et al. 2003; Veranth, Seshadri et al. 2003). Both studies used towers equipped with continuous-reading light scattering instruments to measure dust concentration and anemometers to measure wind speed. These data were used to calculate the flux of dust perpendicular to the road. Flux through a plane perpendicular to the road was calculated by integrating the product of wind speed and dust concentration from ground level to the top of the dust cloud. The experiment at U.S. Army Dugway Proving Ground, UT (Veranth, Seshadri et al. 2003) reported that approximately 85% of the dust was removed within 100 m when passing under nighttime conditions across an array of shipping containers simulating buildings in an urban setting. In contrast, the experiment at Ft. Bliss, TX (Etyemezian, Ahonen et al. 2004; Etyemezian, Gillies et al. 2003) showed negligible removal of dust under sunny daytime conditions with flat, sparsely vegetated terrain. Table 1 shows that the major differences between these field studies were the atmospheric stability and the surface roughness. These field results motivated further experimental and computational studies to better quantify the magnitude of near-source deposition as a function of atmospheric stability and surface roughness.

Deposition of Fugitive Dust Particles on Surfaces

Emission factors for paved and unpaved roads, found in the US EPA document AP-42 (EPA 1998), were originally obtained from measurements made 3 or 5 m from industrial haul roads and a limited number of public unpaved roads. These studies were well designed for their intended purpose and were carefully executed, but did not consider the effects of atmospheric stability and surface roughness on dust transport. Airshed models cannot directly simulate particle deposition that takes place on length scales smaller than the resolution of the grid, typically 1-50 km horizontally and 100 - 1000 m vertically. Thus, there is a need for submodels or correlation factors that can predict the net emission factors by correcting for the fraction of initially suspended dust that is actually transported.

Field measurements of dust concentration and wind speed confirm that the dust flux immediately downwind of a road is predominantly near the ground and at a height comparable to the vegetation, fences, buildings, and similar surface roughness elements (Veranth, Seshadri et al. 2003). The terms impact zone, transition zone, and well mixed zone describe the changes in the vertical profile of the dust cloud downwind of a road (Etyemezian, Gillies et al. 2003). In contrast, for the well-mixed zone the dust concentration is approximately constant throughout the atmospheric mixing height but decreases rapidly near the ground. Gravity settling from a well-mixed cloud is not sufficient to remove a significant fraction of PM_{10} particles on a time scale of a few minutes, but impaction and interception may cause significant removal when most of the dust flux is below the top of the roughness elements.

Experimental data for dry deposition of particles from the atmosphere is often expressed in terms of the quantity (Seinfeld and Pandis, 1998):

$$V_d = \frac{M_{dep}}{\bar{c}At} \tag{1}$$

where,

M_{dep} = Mass deposited on the surface, mg

A = Area of the surface, m^2;

$\bar{c}$ = Time-averaged aerosol particle concentration, mg/m^3;

t = Collection time, s;

which has the dimensions of length/time and is therefore referred to as "deposition velocity." However, this equation is ambiguous when dealing with deposition of particles on real surfaces, such a living plants. The projected area of a plant in the horizontal or vertical plane is much less than the area obtained by summing the surface areas of the leaves and branches. The estimated surface area of these biological structures depends on the minimum length scales that are considered, and greatly increases if the calculation includes small scale features such as leaf hairs and pores. This problem can be resolved by rearranging the equation and expressing quantities on a control volume basis as follows:

$$V_d A_v = \frac{m_{dep}}{\bar{c}t} \tag{2}$$

where,

m_{dep} = Mass deposited within the control volume, mg/m^3;

A_v = Surface area within the control volume, m^2/m^3.

Equation 2 expresses the deposition in terms of a single parameter, referred to as the clearance frequency, with dimensions of s^{-1}. The quantities on the right hand side of the equation can be directly measured in an experiment as described below. The clearance frequency can physically be interpreted as the fraction of particles in the control volume that would be removed per second at the initial rate.

Literature Values for Deposition Velocity

In contrast to the present consideration of near-source deposition in the impact zone, most work on dry deposition of particles from the atmosphere was focused on vertical transfer of pollutants such as sulfate from the well-mixed atmosphere to vegetation that was approximated as a thin layer at the earth surface (Seinfeld and Pandis 1998). The usual formulation by analogy to resistance in an electrical circuit consists of atmospheric, canopy, and boundary layer terms. The flux to the ground is assumed equal to the concentration measured at a reference height multiplied by the mass transfer coefficient. Thus, according to the resistance model

$$F = C(z) v_d(z)$$

where F is the flux of material depositing to the ground (g/m²s) and $C(z)$ is the height-dependent concentration. The deposition velocity is given as the inverse of three resistances in series. That is,

$$v_d = \frac{1}{r_a + r_b + r_c}$$

where r_a is the resistance to aerodynamic transport through the surface layer, r_b is the resistance to transport through the "quasi-laminar sublayer", and r_c is the resistance to collection on vegetative elements. When significant, the effect of gravity can be accounted for in the resistance model by assuming that gravitational settling represents another resistor (r_g) acting in parallel with the combination of r_a, r_b, and r_c. The resistance model for deposition is built on the assumption that close to the ground (i.e. from the top of the surface layer down), the flux of a depositing species is constant with height. Related to the assumption of constant flux, the model also assumes that the system is approximately at steady-state. That is, the concentration profile through the surface and quasi-laminar layers is not changing significantly over time. This corresponds strictly only to the far downwind regime in Figure 1 of part I of the paper (Pardyjak et al. 2007).

The quasi-laminar sublayer resistance must account for several mechanisms that affect particles differently depending on size and flow conditions. Deposition by Brownian diffusion is generally negligibly small for particles larger than about 0.1 μm. Deposition by inertial impaction occurs because a particle is unable to follow the air flow stream around an obstruction and therefore collides and deposits onto the obstruction. The prevalence of deposition by inertial impaction depends on the inertia of the particle, the viscosity of the fluid, and the extent of shearing present in the flow. Particles with aerodynamic diameters larger than about 1 μm are most likely to deposit through this pathway, owing to their inertia. Particles may also deposit by interception whereby the fluid flow field brings a particle into close proximity of an obstruction and the particle adheres to the surface. Since most of the mass associated with dust particles resides with particles larger than 1 μm, inertial impaction and gravitational settling are the primary pathways for dry deposition.

The USEPA Integrated Source Complex 3 (ISC3) model (EPA 1995; Pleim, Venkatram et al. 1984) uses simple flow and particle parameters that are usually available to estimate an appropriate value for r_b. An alternative formulation for deposition velocity using a conductance analogy is provided by Raupach and Leys (1999) Raupach argues that the resistance portion associated with Brownian diffusion scales with the viscous drag (on the surface elements) while the portion associated with impaction scales with the form drag.

Slinn (1982) proposed parameterizations for the three resistances. Though widely cited, the Slinn model is in practice difficult to use owing to the large number of parameters for which measurements are rarely available. A number of investigators have proposed alternative formulations. The aerodynamic resistance is controlled by the amount of vertical mixing within the surface layer; Byun and Dennis (Byun and Dennis 1995) provide a first principles derivation that relies on the Monin Obhukov length scale (L) for turbulence, the roughness height (z_0) and the friction velocity (u_*).

The models of Slinn, Raupach, and others are able, in some cases with the aid of semi-empirical constants and utilization of field and wind tunnel measurements (e.g. (Chamberlain 1967; Wu, Davidson et al. 1992)), to duplicate the characteristic v-shaped curves of deposition velocity vs aerodynamic diameter. However, these models are derived for conditions where the flux through the surface layer is constant. That is, they are generally not applicable to plumes that are in the process of dispersing significantly in the vertical direction and have not yet achieved a quasi time-invariant concentration profile.

The literature data on particle deposition velocity were reviewed and Figure 1 presents values for deposition velocity versus wind speed calculated by the authors from the published equations using the equations and parameters listed in the Supplemental Data. The model by Slinn (1982) has been widely used but it applies to transport from the well-mixed boundary layer to a vegetative canopy, that is to the well-mixed zone. Raupach (Raupach and Leys 1999; Raupach, Woods et al. 2001) studied removal of spray droplets by windbreaks, a case approximated by the impact zone, and developed a correlation that considers the size of the interception elements and the density of the vegetation. Direct comparison between different authors is difficult due to differences in model formulation and the simplifying assumptions. However, it is clear that a wide range of estimates for the magnitude of V_d are found in the literature.

This research addresses quantifying near-source deposition rates for vehicle-generated dust through experimental measurements of deposition on well-characterized artificial surfaces and through application of a quasi-2D transport model (Pardyjak, Speckart et al. 2007) to the reanalysis of field studies measuring dust flux downwind of roads. Actual particle deposition on artificial vegetation and on flat substrates was measured under stable and unstable meteorological conditions. Site conditions from the two downwind dust flux studies were used as the basis for computational simulations that were compared to field measurements.

Methods

Field Studies

The dust flux measurement methods for the Table 1 experiments were previously published (Etyemezian, Ahonen et al. 2004; Etyemezian, Gillies et al. 2003; Veranth, Seshadri et al. 2003). The deposition of vehicle-generated dust on flat substrates and on artificial vegetation adjacent to a road was measured using the experimental setup illustrated in Figure 2. The site conditions and vehicle activity for the two field experiments are summarized in Table 2. The Ft. Bliss experiment was conducted under hot, sunny spring conditions. The Vado Road experiment was conducted under early winter conditions, but the soil moisture was still only 0.7%. Vehicles were driven repeatedly along a test section of unpaved road and a log was kept of the vehicle type, nominal speed, and time of each trip past the instrument station. Dust mass concentration was measured using a DustTrak (TSI Inc., St, Paul MN), which measures light scattering and calculates particle concentration by a proprietary algorithm. A GRIMM Series 1.100 aerosol spectrometer (GRIMM Technologies Inc., Douglasville, GA) measured size-resolved particle number by light scattering. The instrument inlets were placed near the deposition surfaces. Time resolution was 6 s for both the DustTrak and the GRIMM. These instruments provide precise real-time data, but accurate conversion of light scattering data to mass requires a sample-specific adjustment since the particle size distribution, shape, and optical properties may differ from the standard dust used for the manufacturer's calibration. However, the vehicle activity period was too short to collect an adequate filter sample for gravimetric calibration. To avoid artifacts from the uncertainty in the actual mass concentration, the flat substrate data were based on particle number, and mass deposition on artificial vegetation was compared to a control surface to estimate the relative enhancement.

Deposition on Flat Substrates

Collection on flat substrates allowed number-based calculation of deposition velocity by Equation 1 since the collection area and direction were precisely known. A three-axis support stand (Figure 2, middle) was used to hold the sets of six polycarbonate membranes (Millipore type GTTP, Fisher Scientific) taped to the bottom of a 47 mm plastic dish. Substrates faced the ± x, ± y and ± z directions which correspond to streamwise, crosswind and vertical respectively. A standard, right hand coordinate system was used for reference with the direction names being the outward normal vector. The +x direction was facing downwind perpendicular to the road and the +z direction was facing vertical upward. Under field conditions, the wind is seldom perpendicular to the road so there was a wind component in the ± y direction. After exposure in the field, the dish covers were replaced and the samples were taken to the laboratory where a section of each substrate was mounted using conductive double-sided carbon tape, gold coated and imaged with a Hitachi S3000N scanning electron microscope.

Deposition as a function of particle size and direction of the collection surface was determined by using scanning electron microscopy (SEM) to measure and count the particles on the flat substrates. SEM images for counting were taken in a non-overlapping structured grid pattern and sufficient images were made to have 500-1000 particles available for determining the size distribution. Using Scion Image software (Scion Corp., Fredrick, MD) the SEM images were displayed on the computer screen, the particle sizes determined by image analysis, and particles were digitally marked to avoid double counting. To quantify both the infrequent, large, high-mass particles and the abundant, less massive smaller particles, the particles $d>20$ μm were measured on 100X images, particles $5<d<20$ μm were measured on 500X images and particles $0.3<d<5$ μm were measured on 2500X images. The results were compiled in a spreadsheet and mathematically corrected for the relative deposition surface area counted at each magnification. These raw counts were converted into sectional bins corresponding to the particle sizes reported by the GRIMM using a histogram function, V_d was calculated using Equation 1, and data were tabulated by particle size and direction.

Deposition on Artificial Vegetation

Enhanced particle removal caused by flow obstructions in the impact zone was measured using artificial vegetation placed near the edge of the road as shown in Figure 2, bottom. Plastic "fir" Christmas garland was used because the total surface area of the artificial needles and branches could be readily determined and real vegetation is subject to artifacts from natural variation, biogenic debris, and moisture changes. The "fir" created a dense but porous obstruction to the dust flow. Total surface area of the artificial branches and needles was 3.7 m^2 compared to the horizontal projected area of the container, which was 0.18 m^2, and the frontal projected area of the vegetation assembly above the container, which was 0.26 m^2. A control container was used to measure particle settling thorough a horizontal plane in the absence of artificial vegetation. The control and artificial vegetation assemblies were exposed to the vehicle cloud on the downwind side of the road. The deposited material was recovered first by dry shaking and then by water washing. The recovered particles were weighed then separated into four sizes ($d \geq 30$ μm, $10 \leq d < 30$ μm, $3 \leq d < 10$ μm and $d < 3$ μm) by gravity settling in water using the Stokes velocity difference between various size particles. The quality of the gravity settling size separations was verified using SEM, and the fractionated particles were dried and weighed.

Model Simulations

The theoretical development and numerical implementation of a new quasi-2D computational model of near source dust transport and deposition is described in the companion Part 1 paper. (Pardyjak, Speckart et al. 2007) The specific model parameters used in the simulation cases are listed in Table 4 and are discussed as part of the results. The transport and deposition model considers advection, turbulent diffusion, interaction of the surface roughness with the wind field, and particle deposition on both the flat ground surface and on distributed surface area within the canopy height above ground level. The most important site conditions that are included in the model inputs can be summarized in terms of two non-dimensional parameters. The length ratio, H^*, is the ratio of the canopy height to the initial dust cloud height. The time ratio, T^*, is the deposition effectiveness and is the ratio of the time required for a particle to exit the canopy by vertical turbulent transport to the time for the particles to be removed by horizontal deposition onto canopy surfaces. The value of T^* depends on the clearance frequency, the canopy height, and the vertical diffusion coefficient which can be estimated from the wind profile. The model was used in two ways. Inputs were adjusted to fit the model results for dust flux decrease between the source and 100 m to the field measurements and the resulting clearance frequency values were compared to *a priori* expectations. Also, the model was used to predict the effects of alternative site conditions, such as changing atmospheric stability and vegetation canopy roughness, on dust cloud transport and deposition.

Results

The sieve analysis of the surface material from two test roads is presented in Table 3. (Seshadri 2002) Comparing the two entries for Ft. Bliss shows that several days of intense vehicle activity resulted in a decrease of the silt and smaller sand and a relative increase in the coarser sand. Both graded dirt test roads had a finer size distribution than typically specified for the surface fill used on engineered gravel roads, but neither was as fine as pure dry clay.

Particle Deposition

Microscopy counting of particles on the six-directional flat substrate sets showed that particle deposition in the near-source impact zone was reasonably isotropic. Figure 3 gives the directional variation in the deposition velocities normalized by the measurement for the + Z direction (horizontal surface facing up). If gravity settling was the dominant mass transfer mechanism the maximum deposition would be on the +Z surface and all other directions would have negligible deposition. Under the low-wind Vado Road conditions the deposition in different direction ranged from 0.25 to 2 times the deposition on the +Z substrate. The observed enhancement of deposition on the surfaces facing upwind (-X and ±Y) indicates that impaction and interception from advection are major contributors to particle removal. The similar particle counts on the surfaces facing downward (-Z), vertical facing crosswind (+Y) and vertical facing downwind (+X) suggests that small-scale turbulent eddies are also an important deposition mechanism.

Figure 4 shows the particle number-based deposition velocity on flat surfaces as a function of particle size. The data are averaged over all six directions. Comparing these results to the literature correlation equations in Figure 1 suggests that our measurements of deposition on flat surfaces in the near-source impact zone were higher than the Slinn model but within the range of the Raupach model. The two field experiments agree very well in the smaller sizes, but diverge for the $3<d<20$ μm particles. The larger suspended particles may have been systematically undercounted at Ft. Bliss because a longer instrument inlet tube was used for this experiment. Any artifact that lowers the measured suspended aerosol will result in overstating deposition velocity.

The “fir” garland artificial vegetation increased the mass of deposited particles for both the $d<3$ μm and $3<d<10$ μm size ranges compared to the deposition into the control container with the same horizontal surface area. The mass-based results for the clearance frequency, $V_d A_v$, for $3<d<10$ μm particles are shown in Figure 5. The increased clearance resulting from the artificial vegetation suggests that even one small shrub per m^2 can remove a significant fraction of the dust if the cloud stays near the surface for a sufficient time. Although using a light-scattering instrument for dust concentration causes uncertainty in the absolute value of the clearance frequency the relative values for control and artificial vegetation are not dependent on the concentration measurement.

The data in Figures 3-5 suggests that there was a systematic difference between the two deposition experiments. Higher deposition velocity was observed at Ft. Bliss, which had higher wind velocity and atmospheric turbulence compared to the Vado Road experiment. This observed correlation of particle deposition velocity with wind is consistent with the literature summarized in Figure 1.

Model Results

Simulation cases were run using the quasi-2D computational model (Pardyjak, Speckart et al. 2007) to test the hypothesis that differences in atmospheric stability and surface roughness could account for the differences reported by the two field studies at Dugway and Ft. Bliss.

A series of simulations were run treating clearance as an adjustable parameter and using this adjustment to fit the model predictions to the measured downwind dust flux. This process gave fitted values for the clearance frequency of 5 x 10-5 for the Ft. Bliss experiment and 0.22 for the Dugway experiment. These fitted values were then compared to *a priori* expectations. Based on data in Figure 4, the expected deposition velocity for PM_{10} on near-road roughness elements might be from 0.005 to 0.03 m/s. The geometry of common anthropogenic structures (fences and buildings) and natural vegetation, suggests that available surface area at a length scale > 1 mm might range from < 0.1 to > 5 m^2/m^3. Thus, the expected range for clearance frequency is from 5 x 10^{-4} to 0.15 s^{-1}. For the Ft. Bliss experiment the simulations best fitted the experimental data with a clearance of 5 x 10^{-5}. This low value of V_dA_v can be visualized by imagining vegetation, similar to the artificial vegetation assembly shown in Figure 2, spaced on 15 m centers. The Dugway simulation case best fitted experimental data with a clearance frequency of 0.22 s^{-1}. Possible reasons for this high clearance frequency are discussed below. The model explains the observed trends in near-source particle removal but expected values of clearance frequency under predict the range of field observations.

Figure 6 shows the model predictions for the near-source dust cloud shape for the fitted simulations of the Dugway and Ft. Bliss field experiments and for alternative cases representing changed atmospheric stability. The model inputs for the cases are summarized in Table 4. The simulations varied the clearance frequency, Monin-Obukhov length scale, and wind profile equation. The simulation results agree with expectations that an unstable atmosphere results in the dust cloud rapidly growing vertically as seen by comparing the pairs of simulations with the same surface roughness. Likewise the simulations confirm that a large amount of surface roughness results in removing a significant amount of dust from the lower portion of the cloud as seen by comparing the simulations with the same atmospheric stability.

The fitted simulation case for Dugway was further tested by comparing the model predictions for particle concentration, c(x, z, t), to the measurements at each instrument location averaged over the 44 vehicle trips. These results are shown in Figure 7. The dust concentrations varied by over 3 orders of magnitude between the bottom measurement adjacent to the road and the top measurement on the downwind tower. The model predictions for peak dust concentration and for the duration of the passing dust cloud are surprisingly accurate considering the approximations in the model and the sources of error in the measured data. This quantitative agreement gives high confidence in the ability of the model to simulate the interaction of a near-source dust cloud with surface roughness elements. Good agreement is seen at the higher measurement locations. However, the model under predicts the time-integrated near-ground (1-1.7m) dust concentration 30-100 m downwind and the dust cloud at Dugway was wider (took more time to pass the instrument location) than predicted by the model, and the maximum dust concentration downwind was also under predicted. A likely explanation is that the model does not include the large scale recirculating flows which were measured (Nelson, Brown et al. 2004) in the wake of the shipping containers. This increased ground-level dust concentration likely increased the actual dust removal and may explain why a very high clearance frequency (0.22 sec^{-1}) was needed to fit the current model to the measured dust flux at Dugway.

The model was used to study the sensitivity of predicted dust deposition to variations in site conditions. The fraction of the initial dust mass that is still suspended (M_s/M_o) 100 m downwind of the source is most influenced by the ratio of the initial dust cloud height to the roughness canopy height (H*). Figure 8 shows simulation results for the cases listed in Table 4 except that H* was treated as a variable. The field measurements, shown by symbols, are were used to establish the clearance frequency so the model and field data are not independent, rather the model predicts expected trends if canopy height and atmospheric stability are varied. Dust removal is predicted to be significant when the initial dust cloud height is less than the canopy height ($H^* < 1$) and predicted to decrease rapidly when the canopy becomes lower than the initial dust cloud. When the clearance frequency is large, as in the Dugway cases, both canopy height and atmospheric stability have an effect on particle removal. When the clearance frequency is small the atmospheric stability has a negligible effect and the predictions for the two stability conditions coincide. The simulations suggest that the observed dust removal at the Dugway site would have been reduced by either decreased atmospheric stability or by a lower canopy height.

Discussion

This paper contributes to the goal of improving fugitive dust modeling by combining new deposition data with an atmospheric transport theory-based model to reconcile the contrasting results obtained in two recent field studies. There is increasing evidence that fugitive dust emission estimates should be adjusted for the effect on atmospheric stability and surface roughness on the partitioning of the initially emitted dust between long distance transport and near-source deposition. This study suggests that near-source dust removal of vehicle-generated fugitive dust is significant when the canopy height downwind of a road is greater than the initial dust cloud height. Since the initial vehicle-generated dust cloud is on the order of the vehicle height, surface roughness elements greater than 2 m high, such as trees or buildings, many cause significant dust deposition.

The methods used in this study to measure number-based particle deposition are labor intensive, but provide precise, time-resolved data. The data and methods demonstrated in this study can be used for future analysis of field data on horizontal dust flux and to design studies to better quantify the relationship between the configuration of near-ground surfaces and the removal of dust from vehicle-generated clouds. The measurement of particle concentration in the air is a source of uncertainty in the results since the same aerosol mechanisms causing particle deposition on vegetative surfaces also cause instrument inlet and line sampling losses. Our experimental measurements of particle deposition on flat surfaces gives deposition velocities that are an order of magnitude higher than are predicted by the Slinn equation (Slinn 1982), but that are within the range reported by Raupach (Raupach and Leys 1999; Raupach, Woods et al. 2001). The correlations and submodels presented in Figure 1 are simplifications that were derived for different limiting cases. Slinn studied vertical transport from the atmosphere to a horizontal area of forest canopy while the work of Raupach and the data from this study involve deposition from a horizontally moving cloud impinging on the projected area of a surface. Slinn reasoned that because momentum transfer from the wind to ground is higher over a forest, then downward particle transfer should also be higher, and developed a model that used the wind velocity profile in the forest canopy as a parameter. The experiments in this study are more closely analogous to the deposition predicted by models of single fiber filtration efficiency.

Using literature data for atmospheric flow and mixing inputs and using estimates of the clearance frequency that are consistent with experimental data, the quasi-2D model was able to partially explain the differences between the two field experiments that measured dust flux near and 100 m downwind of a road. As shown by Figures 6 and 8, differences in the canopy height, the clearance frequency, and the atmospheric stability account for the difference between <5% dust removal reported for Ft. Bliss and the 85% removal observed at Dugway. The highly simplified Gaussian dispersion model previously used by Etyemezian et al. (Etyemezian, Ahonen et al. 2004; Etyemezian, Gillies et al. 2003) fitted the field experimental data well for the low roughness and unstable atmosphere of the Ft. Bliss experiment but under predicted the measured dust removal for the Dugway experiment. The improved ability to match field measurements, including the detailed time-concentration curves shown in Figure 7, indicate that the new quasi-2D model is a significant improvement over previous computational studies of near-source dust cloud behavior, and that the model captures much of the important physics.

The artificial vegetation experiments demonstrated the usefulness of the technique, but had limitations. Based on Raupach's results the density of "fir" garland used was higher than optimal for dust removal and this probably resulted in flow around rather than through the artificial vegetation. The effect of the collection container on the near-surface air-flow confounds results. An alternative apparatus design would have been to bury the collection container so the rim was flush with the ground surface, but this would have resulted in collecting large amounts of material moving along the ground by saltation, causing a different, and likely greater, artifact.

A major limitation of the current computational model is that there is no basis for predicting the clearance frequency (V_dA_v) *a priori* based on site descriptive data such as vegetation species or the spacing of constructed structures. Developing a submodel for predicting this parameter will require better understanding of small-scale fluid and particle flow dynamics combined with wind tunnel experimentation. Having theoretical or empirical values for clearance frequency under specific site conditions will contribute to the accuracy of regional-scale air quality models since the modeling techniques described in these companion papers can provide near-source deposition corrections for the current fugitive dust emission factors.

Acknowledgements

This work was supported by the Strategic Environmental Research and Development Program project SI-1190, Southwest Consortium for Environmental Research and Policy projects A-02-07, A-04-06, and A-05-05. John G. Watson provide seminal ideas and insights. Richard Countess provided detailed comments on a conference presentation of this work. The contributions of the many University of Texas at El Paso undergraduate students, graduate students Gauri Seshadri, Raed Labban, and Tom Booth, laboratory technician Erin Kaser, and collaborators Ernesto Alfaro-Moreno, Adrian Vasquez, John Walton, Jack Gillies, and Judith Chow are acknowledged.

References

Byun, D. W. and R. Dennis (1995). “Design Artifacts in Eulerian Air Quality Models: Evaluation of the Effects of Layer Thickness and Vertical Profile Correction on Surface Ozone Concentrations.” Atmospheric Environment 29: 105-126.

Chamberlain, A. C. (1967). “Transport of Lycopodium Spores and Other Small Particles to Rough Surfaces.” Proceedings of the Royal Society of London, Series A Mathematical and Physical Sciences 296(1444): 45-60.

Code of Federal Regulations (2006). Code of Federal Regulations, 40CFR51 Subpart P - Protection of Visibility. Government Printing Office,

EPA (1995). User's Guide for the Industrial Source Complex (ISC3) Dispersion Models. Volume II, Description of Algorithms. US Environmental Protection Agency, Office of Planning and Standards,

EPA (1998). AP-42, Chapter 13.2.2 Unpaved Roads. U.S. Environmental Protection Agency, AP-42, Chapter 13.2.2 Unpaved Roads.

Etyemezian, V., S. Ahonen, D. Nikolic, J. Gillies, H. Kuhns, D. Gillette and J. Veranth (2004). “Dust deposition and removal in the arid southwestern United States: measurements and model results.” Journal of the Air & Waste Management Association 54: 1099-1111.

Etyemezian, V., J. Gillies, H. Kuhns, D. Nikolic, J. Watson, J. Veranth, R. Labban, G. Seshadri and D. Gillette (2003). Field Testing and Evaluation of Dust Deposition and Removal Mechanisms: Final Report. Western States Air Resources Council (WESTAR),

Nelson, M. A., M. J. Brown, E. R. Pardyjak and J. C. Klewicki (2004). Area averaged profiles over the mock urban setting test array. Fifth Conference on the Urban Environment, American Meteorological Society, 15.2.

Pardyjak, E. R., S. O. Speckart, F. Yin and J. M. Veranth (2007). “Near-source deposition of vehicle generated fugitive dust on vegetation and buildings. Part 1: Model development and theory.” In Preparation:

Pleim, J., A. Venkatram and R. Yamartino (1984). ADOM/TADAP Model Development Program. Volume 4. The Dry Deposition Module. Ontario Ministry of the Environment, Rexdale, Ontario, Raupach, M. R. and F. L. Leys (1999). The Efficacy of Vegetation in Limiting Spray Drift and Dust Movement. Report Prepared for the Department of Land and Water Conservation, Gunnedah, Australia. CSIRO, Canberra, Australia,

Raupach, M. R., N. Woods, G. Dorr, J. F. Leys and H. A. Cleugh (2001). "The entrapment of particles by windbreaks." Atmospheric Environment 35: 3373-3383.

Seinfeld, J. H. and S. N. Pandis (1998). Atmospheric Chemistry and Physics — From Air Pollution to Climate Change. New York, Wiley.

Seshadri, G. (2002). Fugitive Dust Transport from Unpaved Roads in Arid Climates. MS Thesis,, Department of Chemical and Fuels Engineering, University of Utah,

Slinn, W. G. N. (1982). "Predictions for particle deposition to vegetative canopies." Atmospheric Environment 16(7): 1785-1794.

Veranth, J. M., G. Seshadri and E. Pardyjak (2003). "Vehicle-generated fugitive dust transport: Analytic models and field study." Atmospheric Environment 37(16): 2295-2303.

Watson, J. G. (2002). "Visibility: Science and Regulation." Journal of the Air and Waste Management Association 52(6): 626-713.

Watson, J. G. and J. C. Chow (2000). Reconciling Urban Fugitive Dust Emissions Inventory and Ambient Source Concentration Estimates: Summary of Current Knowledge and Needed Research. Desert Research Institute, DRI Document No. 6110.45.

Western Regional Air Partnership Dust Emissions Forum (2006). Fugitive Dust Handbook. Western Regional Air Partnership, http://www.wrapair.org/forums/dejf/fdh/index.html

Wu, Y. L., C. I. Davidson, D.A. Dolske and S. I. Sherwood (1992). "Dry Deposition of Atmospheric Contaminants: The Relative Importance of Aerodynamic, Boundary Layer, and Surface Resistances." Aerosol Science and Technology 16: 65-81.

Tables

Flux Measurement Experiment	Dugway	Ft. Bliss
Citation	[Veranth, 2003 #1350]	[Etyemezian, 2004 #1414; Etyemezian, 2003 #1377]
Location UTM Coordinates	Northwestern Utah Zone 12 3 14 800 E 44 53 100 N	West Texas Zone 13 3 70 500 E 35 28 100 N
Month	September 2001	April 2002
Time of Day	Night	Afternoon
Atmospheric Stability	Neutral-Stable	Unstable
Surface Roughness	2.5 x 2.5 x 8 m shipping containers simulating buildings	Small sand dunes with sparse 0.1-0.3 m brush
Dust Flux Change	85% decrease	< 5% decrease

Table 1. Published field measurements of dust flux downwind of a test road.

Deposition Velocity Experiment	Vado Road	Ft. Bliss
Location UTM Coordinates	Southern New Mexico 13 3 46 100 E 35 53 900 N	West Texas 13 3 70 500 E 35 28 100 N
Month	November 2002	April 2002
Time of Day	Morning	Afternoon
Atmospheric Stability	Stable	Unstable
Solar Radiation	Overcast	Clear, Sunny
Wind	Calm < 1 m/s (2 mph)	Gusty 6 m/s (14 mph) average
Vehicles	SUV and pickup truck	Sedan, cargo van, heavy military transporter, 18-wheel flatbed
Driving Pattern	Constant nominal speed 30 mph for all trips	Cycle of runs at increasing speeds from 5 -50 mph
Distance from vehicle travel to test surfaces	3 m	5 m
Trips for flat substrates	20	15
Trips for artificial vegetation	50	≅100

Table 2. Field measurements of particle deposition on surfaces.

Site	-3/8 inch	-4 mesh	-20 mesh	-30 mesh	-50 mesh	-100 mesh	-200 mesh
Ft. Bliss, after dust storm	1.00	1.00	0.97	0.85	0.64	0.36	0.07
Ft. Bliss, after extensive driving	0.99	0.98	0.87	0.81	0.59	0.28	0.04
Vado Road	1.00	1.00	0.89	0.79	0.44	0.17	0.08
Construction sand	1.00	0.98	0.71	0.62	0.42	0.05	0.00
Kaolin clay (dry screen)	1.00	1.00	1.00	1.00	0.99	0.72	0.08

Table 3. Sieve analysis of the test road surface material compared to commercial sand and clay. The kaolin is 100% less than 200 mesh by wet screening.

	Dugway Stable (Actual, fitted)	**Dugway Unstable** (Hypothetical, day time)
M-O Length Clearance Frequency Wind model a H* T* u*	55 m 0.22 s^{-1} Equns. 5, 6 in Part 1 0.95 0.8 16.6 0.2 m/s	-55 m 0.22 s^{-1} s^{-1} Equns. 5, 6 in Part 1 0.95 0.8 16.0 0.2 m/s
	Ft. Bliss Stable (Hypothetical, night time)	**Ft. Bliss Unstable** (Actual, fitted)
M-O Length Clearance Frequency Wind model a H* T* u*	100 m $5x10^{-5}$ s^{-1} Equn. 3 in Part 1 Not used 3.0 $2.3*10^{-4}$ 0.3 m/s	-100 m $5x10^{-5}$ s^{-1} Equn. 3 in Part 1 Not used 3.0 $2.3*10^{-5}$ 0.3 m/s

Note: Fetch/initial dust cloud, F* = 2. H* is the ratio of canopy height to initial dust cloud height. T* is defined by Equn. 13 in Part 1. The wind attenuation coefficient, a, appears in Equn. 6 of Part 1 and literature values are summarized in Table 1 and Figure 3 of Part 1.

Table 4. Summary of inputs for the cases shown in Figures 6 and 8.

Supplemental Data

Factors common to all models		
Parameter	**Value**	**Comment**
Wind Speed	Model variable	1 to 10 m/s
Particle Size, D_p	7 µm	Typical mass median of coarse fraction ($PM_{2.5-10}$)
Particle density, ρ_p	2500 kg/m^3	Mineral dust
Air Density, ρ	1.22 kg/m^3	Sea level
Air kinematic viscosity, ν	18x10^{-6} kg m/s	Sea level, 17 °C
Friction Velocity, u^*	u* = 0.06 U	Assumed value
Gravitational Acceleration, g	9.81 m/s^2	
Seinfeld and Pandis Model		Resistance model
Deposition Equation	$v_d = \dfrac{1}{r_a + r_b + r_c} + v_s$	Equn.. 19.2 in {Seinfeld, 1998 #603}
	$r_a = r_c \approx 0$	Assume much less than r_b
	$r_b = \dfrac{1}{\left(Sc^{-2/3} + 10^{\frac{-3}{St}}\right)u^*}$	Equn. 19.18 in {Seinfeld, 1998 #603}
	$St = \dfrac{\left(V_g / g\right)u^{*2}}{\nu}$	Equn. 2-26 in {Etyemezian, 2003 #1377}

Model Parameters		
Schmidt Number	$Sc = \frac{\nu}{D}$	$4.5*10^6$
Brownian diffusivity	$D = \frac{\kappa T C_c}{3\pi\mu D_p}$	$3.3*10^{-12}$ m^2/s
Gravity settling velocity	$V_g = \frac{D_p^2 \rho_p g}{\mu}$	$3.9*10^{-3}$ m/s
Slinn Model		Resistance with canopy effects
Deposition relationship	v_d from Figure 5 in {Slinn, 1982 #1203}	Lookup using empirical chart based on Chamberlain data. {Chamberlain, 1967 #1376} Wind speeds interpolated using Equn. 30 in {Slinn, 1982 #1203}
Canopy parameter	γ = 1.5 and 3.5	Expected range 2 - 5 per {Slinn, 1982 #1203}
Velocity at reference height	u_r= U	Wind speed variable.
Raupach Model		Deposition on windbreaks.
Deposition Equation	$v_d = \left(\frac{St}{St + p}\right)^q U$	Rearranged Equn. 2 in {Raupach, 2001 #1374}
Stokes number	$St = \frac{\rho_p d_p^2}{18\rho_a \nu_a \, {}^{d_e}\!/\!_{2U}}$	
Interception element length scale	d_e - 0.001 and 0.01 m	1 mm and 10 mm elements intercepting air flow.
Coefficient p	0.8	Recommended value in {Raupach, 2001 #1374}
Coefficient q	2	Recommended value in {Raupach, 2001 #1374}

Supplemental Table 1. Model citations, equations, and parameters used by the authors to calculate deposition velocity versus wind speed in Figure 2.

Figures

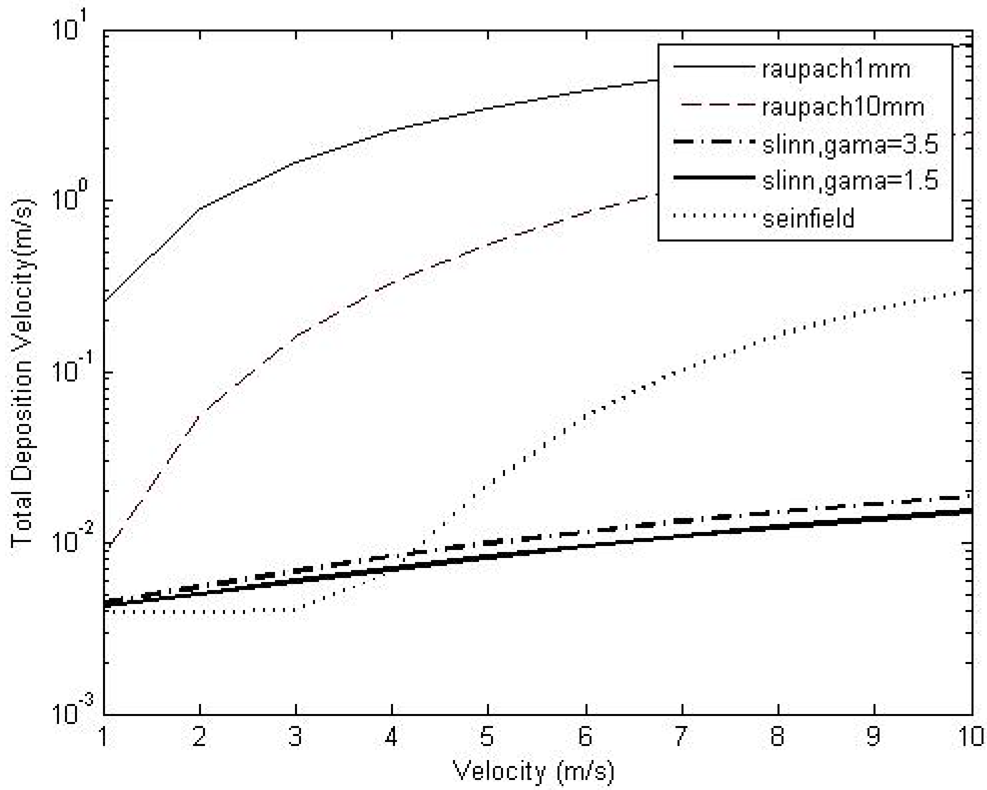

Figure 1. There is a large variation in the predicted values for deposition velocity versus wind speed. Curves were calculated by the authors using equations from the literature. {Raupach, 2001 #1374; Seinfeld, 1998 #603; Slinn, 1982 #1203} Model deposition velocity equations and parameter numerical values used to generate the curves are listed in the Supplemental Data, Table S1.

Figure 2. Top - Field measurement of deposition velocity of vehicle-generated dust near an unpaved road. Middle - Detail of directional flat substrates prior to removal of the covers for collection. Bottom - Detail of the plastic fir garland artificial vegetation assembly and the control tub prior to removal of cover.

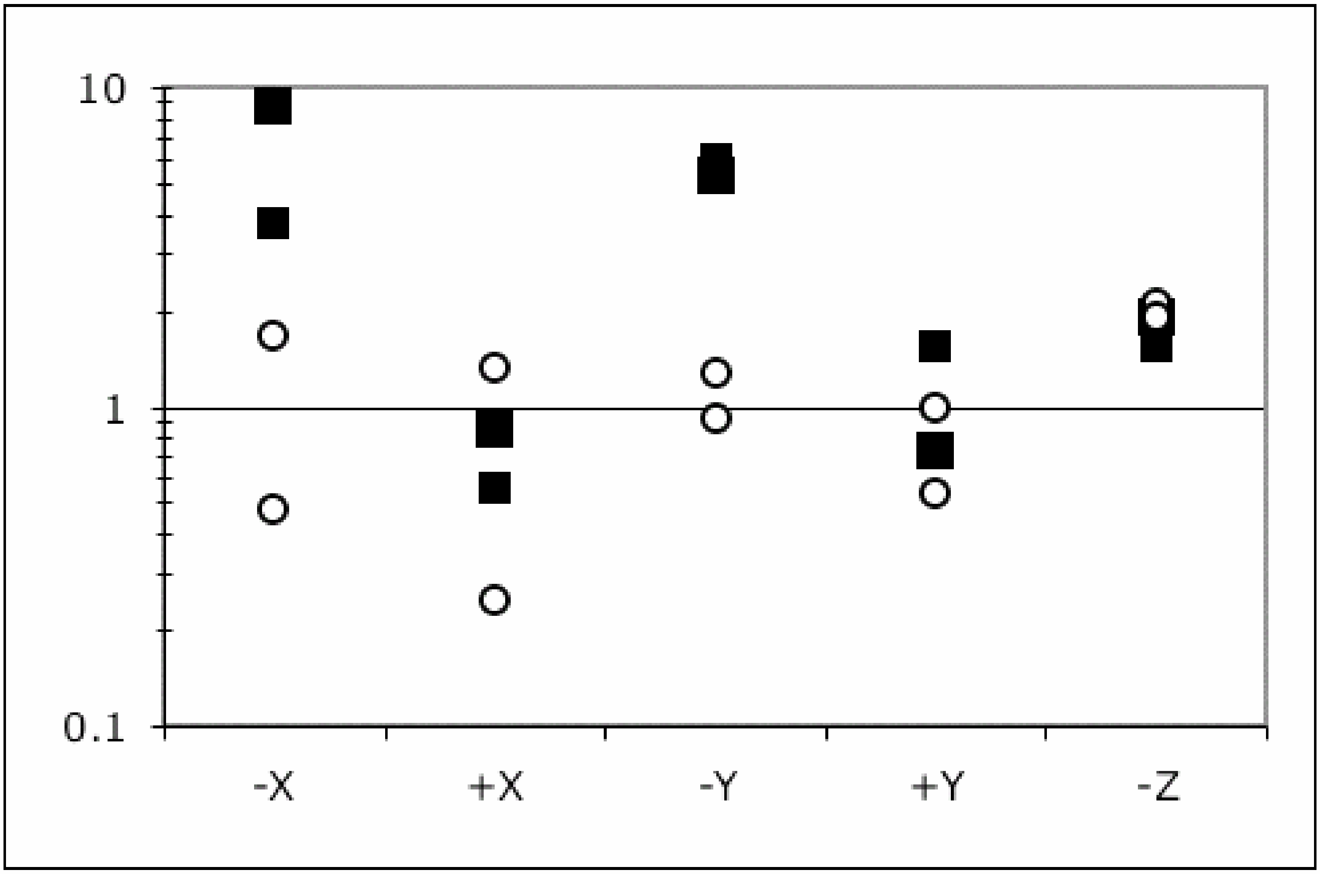

Figure 3. Directional deposition velocity from two independent sets of directional substrates measurements at each site: Ft Bliss (black squares, ■) and Vado Road (open circle, ○). Data are normalized by the deposition velocity for the +Z (horizontal facing up) direction. Deposition is enhanced on the surfaces facing upwind or crosswind (-X and -Y at Ft Bliss) and deposition is nearly isotropic under low wind conditions encountered at Vado Road.

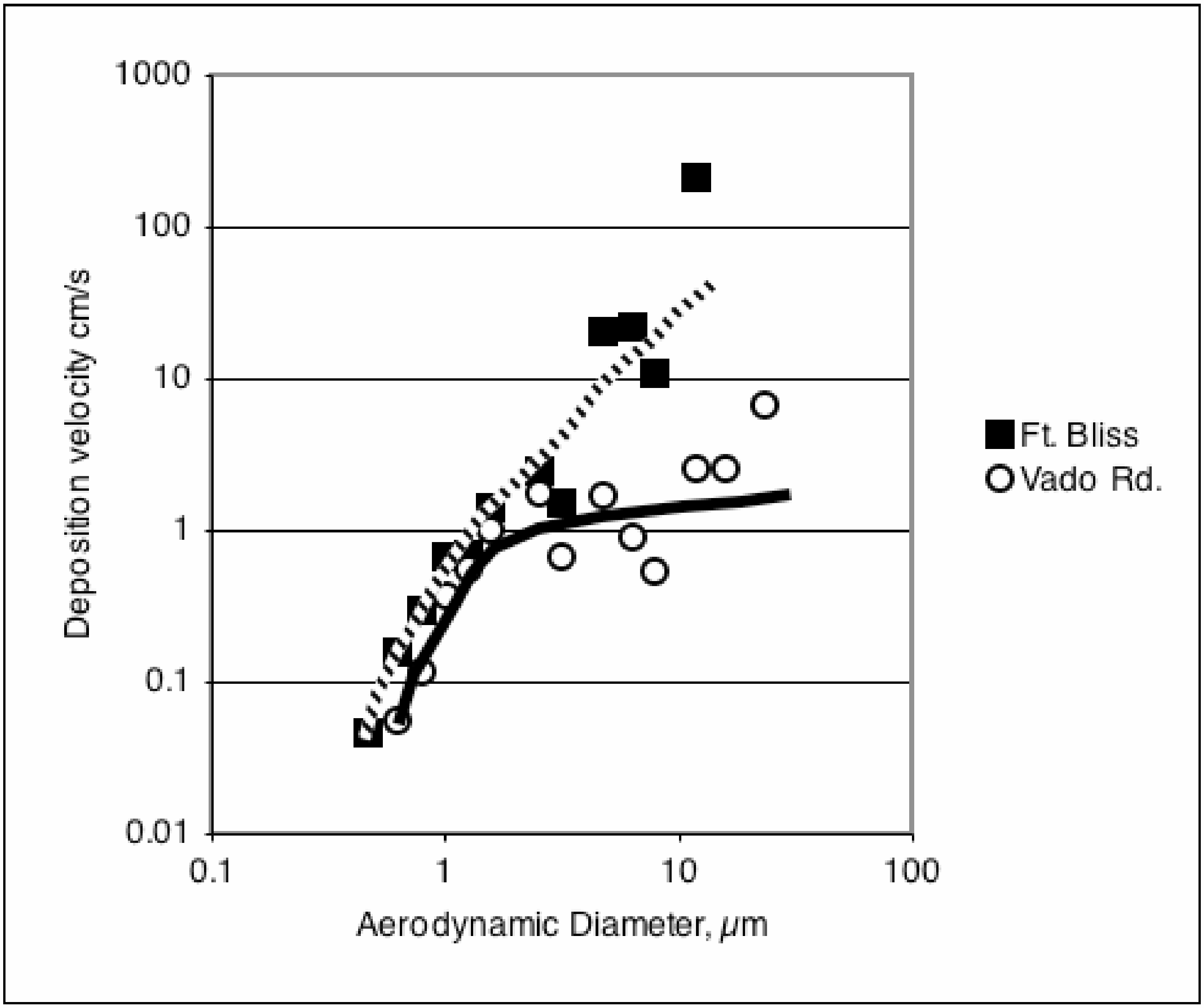

Figure 4. Deposition velocity versus aerodynamic diameter based on particle number data from two field experiments using flat substrates. Results are an average over all six directions.

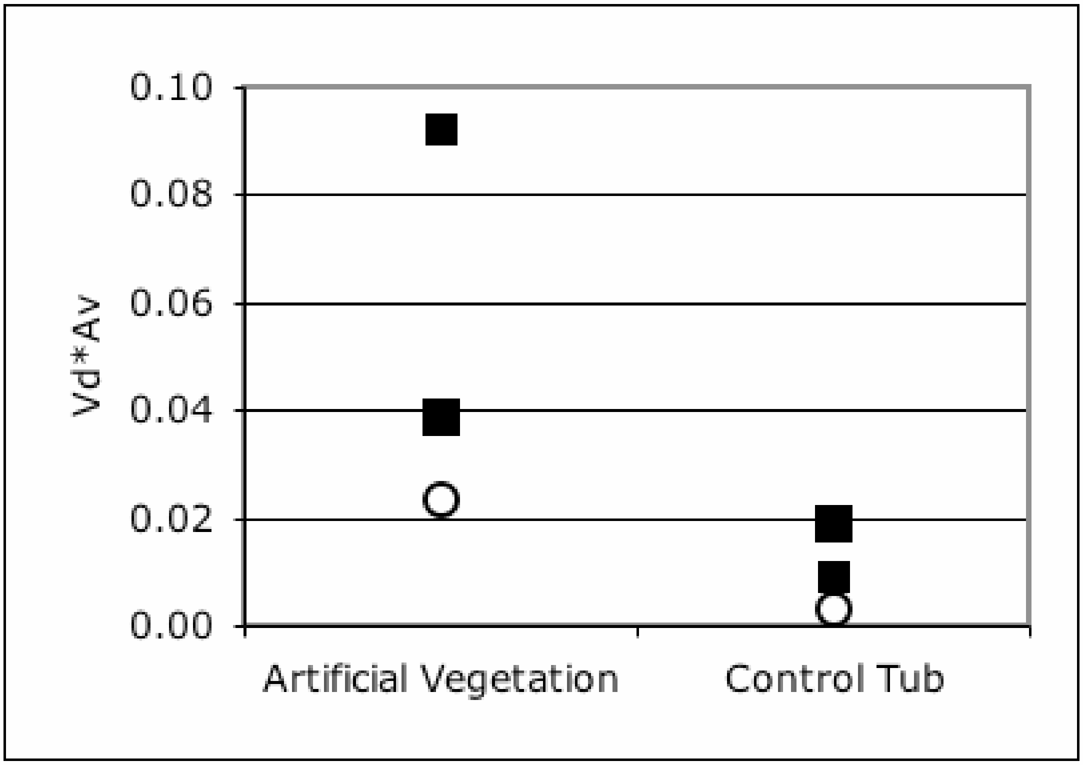

Figure 5. Artificial vegetation enhanced the deposition of 3 < d < 10 µm particles compared to the control flat surface. Data are the clearance frequency (s^{-1}) calculated by Equation 2 for two days at Ft Bliss (black squares, ■) and one day at Vado Road (open circle, ○).

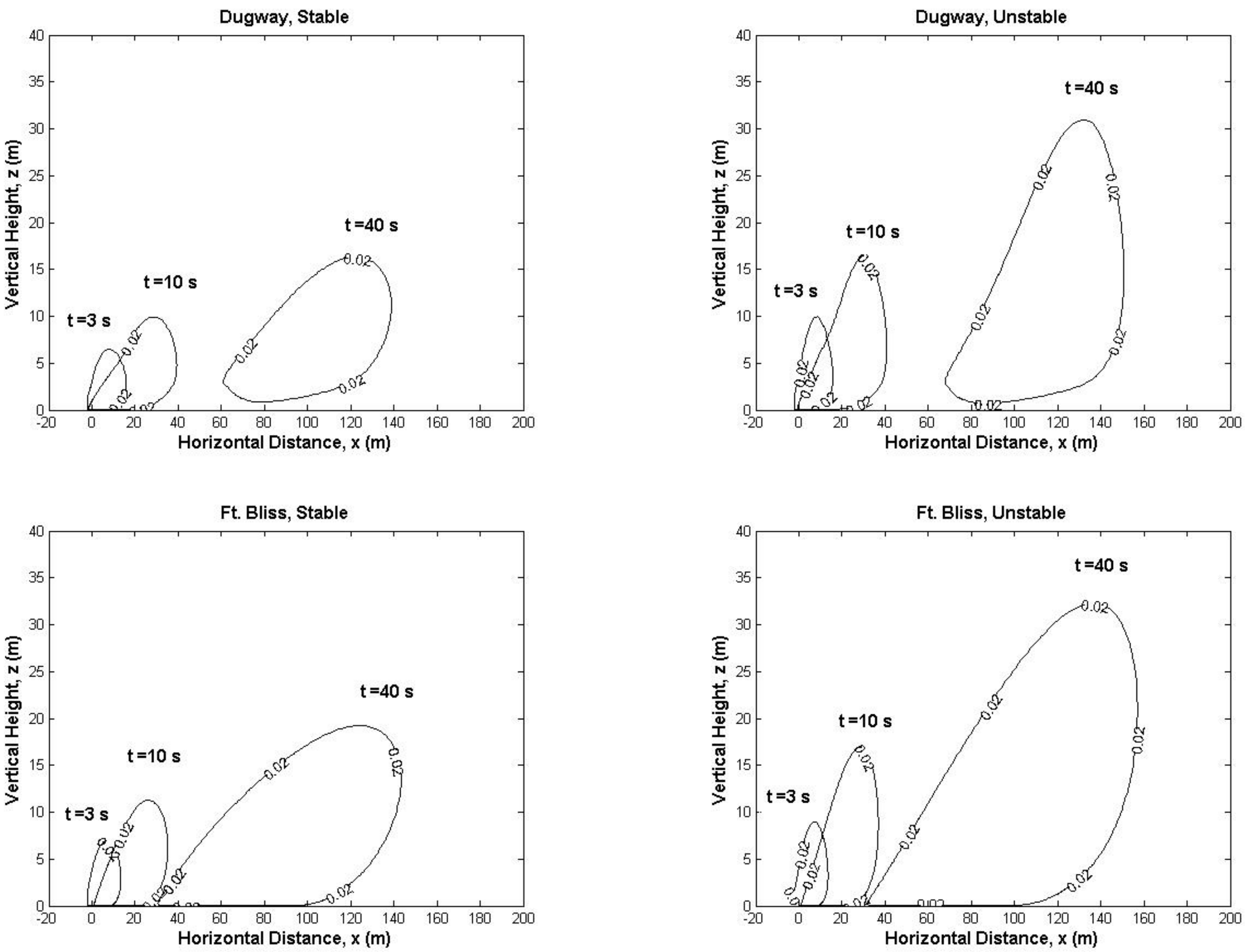

Figure 6. Model simulations showing the shape of the dust cloud versus time for actual and hypothetical cases with the inputs summarized in Table 4. The contour represents 0.03% of initial dust cloud concentration.

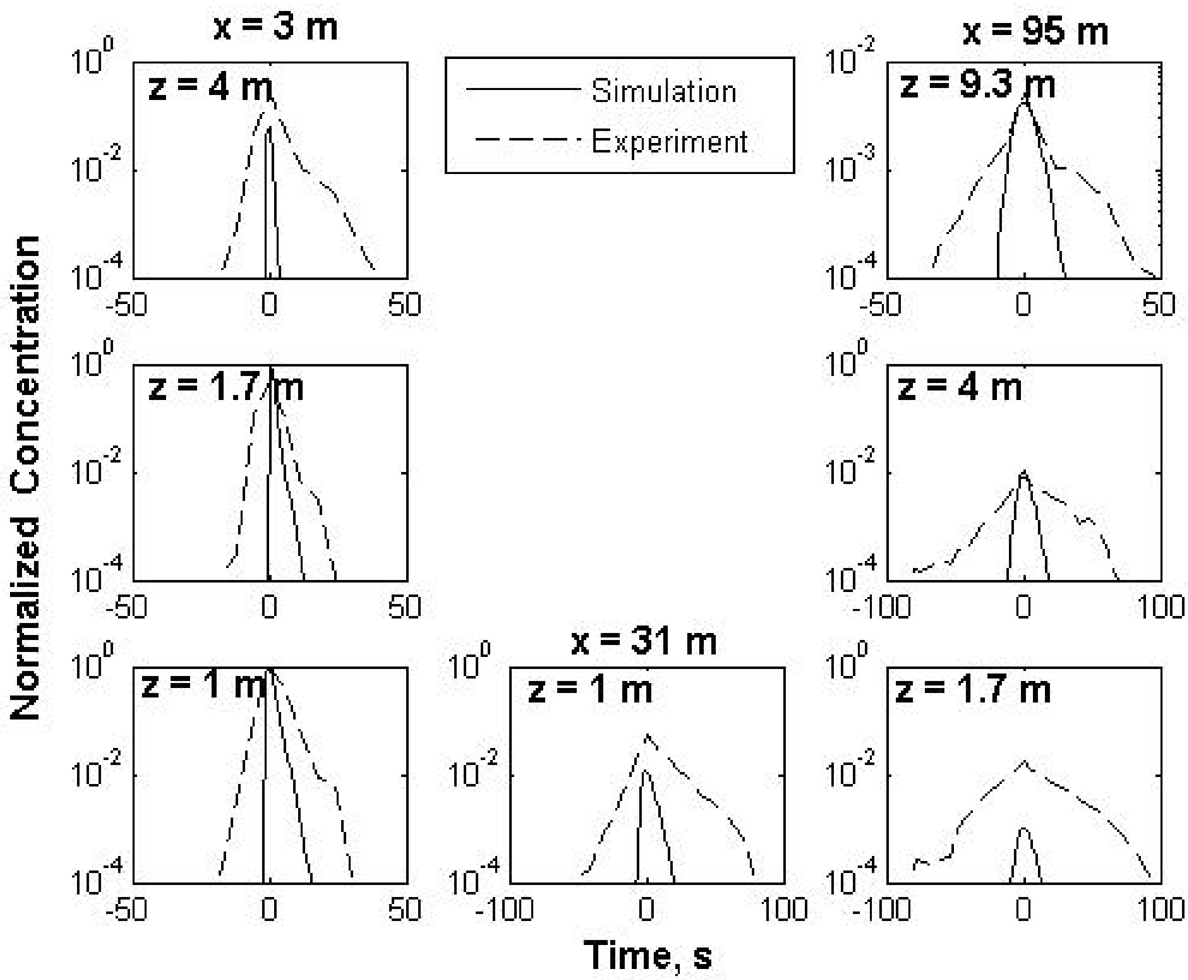

Figure 7. Comparison of simulation results with the field data at the instrument locations used in the Dugway field study. Experimental and simulation concentration data are normalized so that the maximum concentration is unity at the 3 m downwind 1 m high location and time data are aligned so that t = 0 represents the time of peak concentration at each location.

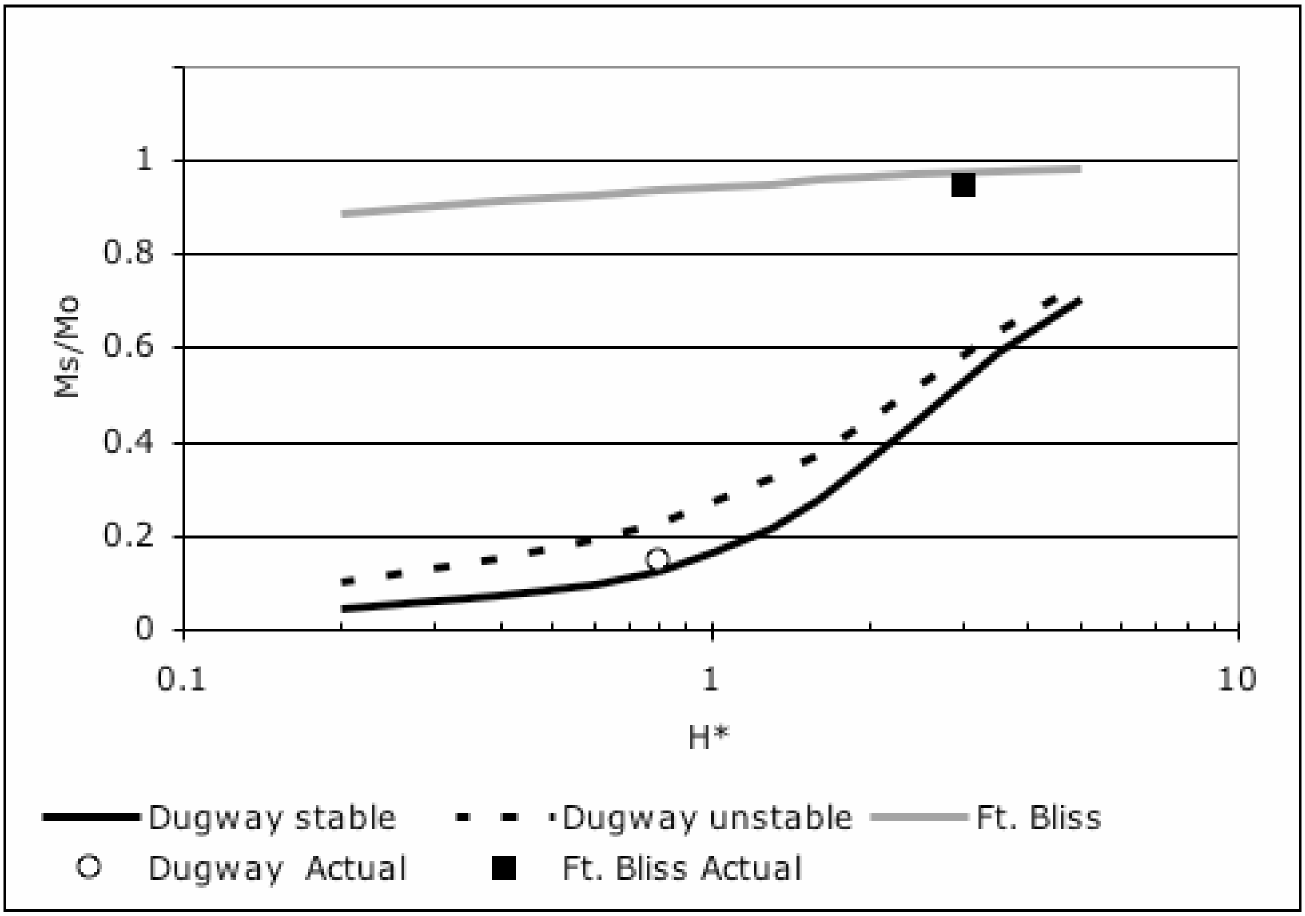

Figure 8. Model predictions and experimental measurements for the fraction of the initial dust mass remaining suspended at 100 m downwind versus non-dimensional height (H* = initial dust cloud height/canopy height). Case-specific model input parameters other than H* are the same as in Table 4.